ANALYSIS OF THE ATMOSPHERIC MIXED LAYER OVER THE WESTERN PACIFIC WARM POOL

by

Jennifer A. Dickey

Research supported by the National Oceanic and Atmospheric Administration under Grant NA37RJ0202

Colorado State University

DEPARTMENT OF ATMOSPHERIC SCIENCE

PAPER NO. 609

ANALYSIS OF THE ATMOSPHERIC MIXED LAYER OVER THE WESTERN PACIFIC WARM POOL

by

Jennifer A. Dickey

Department of Atmospheric Science
Colorado State University
Fort Collins, CO 80523

Summer 1996

Atmospheric Science Paper No. 609

ABSTRACT

ANALYSIS OF THE ATMOSPHERIC MIXED LAYER OVER THE WESTERN PACIFIC WARM POOL

Knowledge of the atmospheric mixed layer is fundamental to understanding the ocean-atmosphere coupling over the western Pacific warm pool. In this study, we use rawinsonde data from the Tropical Ocean Global Atmosphere (TOGA) Coupled Ocean Atmosphere Response Experiment (COARE) to determine the depth of the atmospheric mixed layer over the warm pool region.

Mixed layer properties (depth, potential temperature, and specific humidity) are investigated for four sounding sites: Kapingamarangi, *Shyian 3*, *Xiangyanghong 5*, and the *Moana Wave*. Time series from the four-month Intensive Observation Period (IOP) illustrate the long-term variability of the mixed layer. Frequent convection during COARE substantially modified the atmospheric boundary layer over a wide range of time scales (hours to weeks). These time series show that periods of strong surface winds and precipitation tend to correspond to shallow mixed layers, emphasizing the impact of convection.

To investigate the mixed layer during relatively undisturbed periods we studied various light-wind cases. Histograms of mixed layer depth for light-wind periods show a more normal (Gaussian) distribution than those that include precipitation events. The mixed layer is deeper during both light-wind periods and the westerly wind bursts (after precipitation has ended).

The mean mixed layer depth at the four stations analyzed ranged from 470 m to 540 m. These values are consistent with the mean mixed layer depth over other regions of the tropics,

despite the larger average surface fluxes over the warm pool. For example, Fitzjarrald and Garstang (1981) found the mean mixed layer depth in the Atlantic to be 424 m while Bond (1992) concluded that it was approximately 500 m in the eastern equatorial Pacific.

The possibility of a diurnal variation in the atmospheric boundary layer directly above the ocean has typically been discounted due to the relatively small variation in the tropical sea surface temperatures (SSTs). However, a perceptible variation in the boundary layer over the equatorial western Pacific is evident using TOGA COARE sounding data. The mixed layer depth over Kapingamarangi exhibited a diurnal cycle that was maximized under clear skies and light-wind conditions with the depth varying approximately 16.5% throughout the day. Potential temperature and specific humidity within the mixed layer also demonstrated diurnal cycles (with amplitudes of approximately 0.7°K and 0.4g/kg respectively).

Similar diurnal variations in the mixed layer depth were found at other sounding stations in the Intensive Flux Array (IFA). The depth varied 7.6% at the *Moana Wave*, and 13.0% at both *Shyian 3*, and *Xiangyanghong 5*. The slightly larger variation in the mixed layer depth at Kapingamarangi may be due to a small land effect from the atoll.

This study has provided a better understanding of the atmospheric mixed layer over the western Pacific warm pool. The behavior of the atmospheric mixed layer is an essential factor in the coupling between the atmosphere and the ocean. An understanding of this coupling is instrumental in improving the boundary layer parameterizations and global climate modeling.

ACKNOWLEDGMENTS

I would like to thank my advisor, Dr. Richard Johnson, for his guidance and advice throughout my research. His patience and enthusiasm towards my work made my masters experience an enjoyable one. I would also like to thank the members of my committee, Dr. William Gray and Dr. Steve Robinson for their time and input. A special thank you to Paul Ciesielski for his abundant help with various computer programs and graphics and to Rick Taft for keeping my computer running. Finally, I would like to thank Gail Cordova for helping assemble the final product.

This research has been supported by the National Oceanic and Atmospheric Administration under Grant NA37RJ0202.

TABLE OF CONTENTS

LIST OF ACRYONMS

TOGA	Tropical Ocean Global Atmosphere
COARE	Coupled Ocean Atmosphere Response Experiment
IOP	Intensive Observation Period
GATE	GARP Atlantic Tropical Experiment
IFA	Intensive Flux Array
ENSO	El Niño - Southern Oscillation
SST	Sea Surface Temperature
ATEX	Atlantic Tradewind Experiment
BOMEX	Barbados Oceanographic and Meteorological Experiment
ISS	Integrated Sounding System
NCAR	National Center for Atmospheric Research
NOAA	National Oceanographic and Atmospheric Administration
PAM	Portable Automated Mesonet
RASS	Radio Acoustic Sounding System
LSA	Large Scale Array
OSA	Outer Sounding Array
IMET	Improved METeorology
WHOI	Woods Hole Institute
RH	Relative Humidity
BLIS	Boundary Layer Instrumentation System
MCS	Mesoscale Convective System
UTC	Universal Time Coordinate
LCL	Lifting Condensation Level
GMS	Geostationary Meteorological Satellite

LIST OF SYMBOLS

θ	potential temperature
q	specific humidity
z_i	mixed layer top (height of the inversion)
z_t	entrainment zone top
θ_v	virtual potential temperature
Δ	inversion strength
γ	lapse rate
w	vertical velocity
F	buoyancy flux
E	evaporation
B	Bowen Ratio
c_p	specific heat at constant pressure
L_v	latent heat of vaporization
T	temperature
v	wind speed
z_s	surface layer top
Q_{Rm}	vertically integrated radiative heating
e	vapor pressure
T_k	absolute temperature
p	pressure
Γ	dry adiabatic lapse rate
z_b	cloud base height
U	wind speed

Chapter 1

INTRODUCTION

The global climate system is sensitive to processes that occur in the western Pacific warm pool. These processes are highly dependent on the atmospheric and oceanic boundary layers and the interface between the two. One of the main objectives of the Tropical Ocean Global Atmosphere (TOGA) Coupled Ocean-Atmosphere Response Experiment (COARE) was to study the ocean-atmosphere coupling in the warm pool region. The results may aid, among other things, the on-going effort to understand and predict climate change as well as the El Niño-Southern Oscillation (ENSO) phenomenon. Despite the importance of this region, little is known about the mean structure of the atmospheric boundary layer over the warm pool and its modulation by convection on short and long time scales. Oceanographers have discovered a diurnal cycle in sea surface temperature (SST) (Weller and Anderson 1995); however, its impact on the atmospheric mixed layer has not yet been documented.

The purpose of this study is to address some of these questions through an analysis of the atmospheric mixed layer over the western Pacific warm pool using TOGA COARE sounding data. Since the ocean-atmosphere coupling occurs through the mixed layer, an understanding of this level is fundamental to the goals of TOGA COARE. Like the hitch between two railroad cars, the oceanic and atmospheric mixed layers link two large, independent masses that synergically modify the global climate and may even determine the success of such things as the Peruvian fishing industry. To elucidate the role of the mixed layer in this much larger scheme, we will study the variability of the mixed layer in relation to surrounding atmospheric conditions. Of specific importance is the characterization of the mixed layer response to deep convection on

short- and long-term time scales. In addition, we analyze the diurnal cycle of the atmospheric mixed layer depth to determine if there is a complement to the diurnal cycle found in the SST. An analysis of this daily variation offers additional insight to the sensitivity of the mixed layer to its environment. The resulting information is important in order to develop models that accurately simulate the warm pool and to obtain a better understanding of global climate change, the El Niño-Southern Oscillation, and the intraseasonal variability of the coupled ocean-atmosphere system (Webster and Lukas 1992).

Chapter 2

BACKGROUND AND LITERATURE

2.1 Background

Stull (1993) defines the atmospheric boundary layer as the part of the troposphere that is directly affected by the earth's surface and responds to surface forcing with a time scale of an hour or less. The part of the boundary layer where turbulent mixing occurs is called the mixed layer. The surface layer, which may or may not be a part of the mixed layer, is the lowest region where turbulent fluxes and stress vary by less than 10% of their magnitude (Stull 1993).

The mixed layer itself is produced by turbulent eddies. These eddies may be the result of heating from below or cooling from above. In the former case, warm air rises from the radiatively heated surface until it encounters the stable air that caps the mixed layer. If clouds form, their tops will radiatively cool creating cold thermals that sink. Both processes -- air rising and sinking -- can also occur simultaneously. This turbulence creates a vertically uniform distribution of heat, moisture, and momentum (Stull 1993).

Soundings of the mixed layer typically show a shallow, unstable surface layer beneath an almost perfectly vertical profile of potential temperature (θ) and specific humidity (q) where mixing is occurring, although the structure over water can be somewhat different from that over land. The mixed layer is capped by an entrainment zone where the potential temperature increases with height and the moisture decreases. In this layer, laminar air from the free atmosphere is entrained into the region of turbulent flow. Thus, the entrainment zone is the transition between turbulent flow in the mixed layer and laminar flow in the free atmosphere.

In general, the depth of the marine atmospheric boundary layer varies little over time in moderate to strong wind conditions compared to the variation over a heated land surface. Strong turbulence in the mixed layer keeps the sea surface temperatures relatively constant while the large heat capacity of the ocean allows it to absorb heat from the sun without substantially altering its temperature. Thus, one would expect that the SSTs change little, if any, throughout the day. However, data from the western Pacific show a distinctive diurnal variation in the SSTs at times when the winds become light (Weller and Anderson 1995). This variation suggests the possibility of a similar diurnal variation in the atmospheric mixed layer above the ocean surface.

The boundary layer over land is far more variable than over the ocean. Unlike the ocean, land cannot store energy. The ground warms and cools in response to solar radiation. Additional forcing from evaporation and transpiration, pollutant emission, and terrain induced flow modification also contribute to changes in the boundary layer thickness. Over land, this can range from hundreds of meters to a few kilometers. Since the boundary layer over land responds so quickly to solar radiation there is a distinctive diurnal variation. Note, the boundary layer itself absorbs very little solar radiation. The radiation is transmitted to the ground which then warms and forces changes in the boundary layer above.

When precipitating convection occurs, the boundary layer is disrupted by downdrafts. Since the western Pacific warm pool is an area of abundant rainfall, this disruption is frequent and vigorous.

2.2 Literature Review

In the tropics, the boundary layer is often referred to as that layer containing both the mixed layer and the tradewind cumulus layer. In this more general context, traditional theory characterized the tropical boundary layer as sloping dramatically upward from the subtropics to the intertropical convergence zone. Ekman theory also suggests that the boundary layer depth

grows in the equatorial region due to the small Coriolis parameter. However, Gray (1972) found that rotation does not appear to be a factor in determining the depth of the boundary layer. In contrast to theory, his observations did not show an increase in the thickness of the boundary layer towards the equator. More recent work by Schubert et al. (1995) investigated the dynamical adjustments of a tradewind inversion layer of variable strength and depth. Their solution revealed that the subtropical inversion height dynamically extends into the tropics causing little variation in the depth of the boundary layer towards the equator.

Due to the lack of data over the tropical oceans, there have been few opportunities to study the marine boundary layer in any detail. Furthermore, results from experiments in the Atlantic, for example, may differ substantially from those over the western Pacific warm pool or any other region exhibiting unique characteristics. Among the experiments conducted over tropical oceans were the Atlantic Tradewind Experiment (ATEX) and the Barbados Oceanographic and Meteorological Experiment (BOMEX) (Augstein et al. 1974; Holland and Rasmusson 1973). The 1974 GARP Atlantic Tropical Experiment (GATE) provided extensive boundary layer measurements over the tropical ocean. GATE utilized the Boundary Layer Instrumentation System (BLIS) that measured the velocity field, temperature, humidity, and pressure and offered the luxury of greater time resolution than conventional radiosondes (Fitzjarrald and Garstang 1981).

Another approach to studying the atmosphere over the tropical oceans is to use aircraft measurements. LeMone and Pennell (1975) used aircraft data to study the relationship between cloud distribution and the subcloud layer structure and fluxes in non-precipitation systems. They looked at three cases that occurred on December 14 and 15, 1972 north of Puerto Rico. Their results showed a distinct connection between the subcloud fluxes and the cloud distribution. In the highly suppressed cases, LeMone and Pennell (1975) found that subcloud layer roll vortices determined the location of the clouds. When deeper cumulus convection was present, they found

strong, cloud-scale updrafts linking the individual cumulus to the subcloud layer. In their mean profiles, LeMone and Pennell (1975) found the mixed layer top (z_i) to be approximately 600 m. They also found that the temperature flux is negative at the top of the mixed layer due to the entrainment of warmer, drier air from above.

Fitzjarrald and Garstang (1981) were among those who studied the tropical boundary layer using the GATE data. Their study included an analysis of the atmospheric mixed layer and its structure during both heavy convection and light to moderate precipitation events. They found the overall mixed layer top in GATE to be 424 m, substantially less than LeMone and Pennell (1975) who studied only fair-weather cases. They concluded that disturbed mixed layers are shallower and cooler than undisturbed ones. Furthermore, although light rainfall may moisten the mixed layer, mixed layers adjacent to strong rainfall were found to be drier. This is possibly due to the dry downdrafts from the convective region spreading out laterally. Fitzjarrald and Garstang (1981) also show how drying in the upper boundary layer may lead to deeper mixed layers.

The GATE data offered valuable insight to the properties of the atmosphere over the tropical ocean. However, the western Pacific warm pool region boasts the warmest SSTs in the open oceans as well as the largest annual precipitation and latent heat release in the atmosphere (Webster and Lukas 1992). The information obtained from the Atlantic may or may not be representative of the tropical atmosphere in the warm pool region. Since the western Pacific plays an important role in the global climate system, including the ENSO phenomenon, an in-depth study of the region was necessary to fully understand the processes at work.

The goals and design of TOGA COARE were detailed in Webster and Lukas (1992). In their article, Webster and Lukas (1992) outline the four scientific goals of COARE as to describe and understand: 1) the principal processes responsible for the coupling of the ocean and the atmosphere in the western Pacific warm pool system; 2) the principal atmospheric processes that

organize convection in the warm pool region; 3) the oceanic response to combined buoyancy and wind-stress forcing in the western Pacific warm pool region; and 4) the multiple-scale interactions that extend the oceanic and atmospheric influence of the western Pacific warm pool system to other regions and vice-versa. Webster and Lukas (1992) expand on these goals and describe the design of the experiment that incorporated several measurement systems on various platforms. Satellite, aircraft, ships, and land-based stations provided an assortment of data from various vantage points. Weller and Anderson (1995) explored one of these platforms by looking at numerous time series from the Improved METeorology (IMET) buoy in center of the TOGA COARE region. Their goal was to attain a more complete description of the air-sea fluxes in the warm pool region in order to better understand the atmosphere-ocean coupling. Among their observations was a strong diurnal variation in the sea surface temperature. This variation was most pronounced during periods of low wind speeds with the strongest case having an amplitude of 3°C and typical means ranging from 0.5 to 2.0°C.

The Integrated Sounding System (ISS) used in TOGA COARE is described in detail in an article by Parsons et al. (1994). They discuss the goals of the ISS and describe the instruments that comprise the system. Their article also shows various examples of the data obtained by the ISS in order to show how remote and in situ instruments can be integrated to obtain data in a tropical atmosphere. In one example, they used data collected from a shipboard ISS to examine a strong convective outflow that produced a surface temperature fall of 4°C and enhanced the ocean heat fluxes by four times.

Convective outflows proved to have a large impact on the boundary layer in TOGA COARE. However, convective downdrafts are not exclusive to the warm pool region. Multiple studies have looked at convective wakes and their effect on the tropical boundary layer. Using acoustic sounder facsimile data from GATE, Gaynor and Ropelewski (1979) divided the boundary layer into three categories: undisturbed, early perturbed (density current), and mature

perturbed (wake). They then analyzed the dynamic and thermodynamic modifications on the boundary layer by precipitation and convection. Johnson and Nicholls (1983) used rawindsonde data from GATE to study the effects of a tropical squall line on the atmospheric boundary layer. More recently, Young and Perugini (1995) used TOGA COARE data to look at convective wakes in the equatorial western Pacific. Although each study had a unique perspective on convective wakes and how they effect the boundary layer, the final results (which are discussed in Chapter 4) were all very similar.

To further understand the processes that affect the atmospheric boundary layer, this study analyzes the mixed layer over the warm pool region. The opportunity to study the mixed layer over the warm pool is unique in that TOGA COARE provided the first measurements detailed enough to resolve mixed layer information ranging from long-term variability to diurnal cycles in this area. As the link between the ocean and the atmosphere, the mixed layer is an important factor in understanding the warm pool's role in the global climate system.

Chapter 3

DATA AND ANALYSIS

3.1 Basic Data Field

The TOGA COARE Intensive Observing Period (IOP) lasted four months from November 1, 1992 to February 28, 1993. TOGA COARE employed an Integrated Sounding System (ISS) that was developed jointly by the National Center for Atmospheric Research (NCAR) and the National Oceanic and Atmospheric Administration (NOAA). The ISS incorporated various in situ and remote measurement systems taking advantage of the positive attributes of each (Miller and Riddle 1994). The instrumentation consisted of four separate subsystems: 1) Omegasondes, 2) 915 MHz Doppler clear-air wind profilers, 3) Radio Acoustic Sounding Systems (RASS), and 4) surface Portable Automated Mesonet (PAM) stations (Parsons et al. 1994).

The ISS sounding system was a standard NCAR "CLASS" system that used a Vaisala RS 80-15 N type H radiosonde and an Omega windfinding system (Miller and Riddle 1994). TOGA COARE sounding information includes a "ten-second" data set and an "interpolated" data set (Loehrer et al. 1996). Ten-second sounding data contained thermodynamic, horizontal wind, and position information. The interpolated data set was computed from the ten-second data by linearly interpolating between the data points at constant pressure increments of 5 mb . The 5 mb data have comparable resolution to the ten-second data in the low levels since the balloon ascended at approximately 5 m/s and data were recorded every 10 s (at low levels 100 m ~ 10 mb). We used the 5 mb interpolated sounding data in this study. The 5 mb data provided

adequate resolution to analyze the structure of the boundary layer including the top of the mixed layer and the entrainment zone.

The TOGA COARE sounding network over the equatorial western Pacific consisted of three nested arrays designed to study properties of the atmosphere in the warm pool region. The Large Scale Array (LSA), located from 140° E to 180° E, 10° S to 10° N, studied synoptic scale features with soundings released twice-per-day (Figure 3.1). The Outer Sounding Array (OSA) and the Intensive Flux Array (IFA) studied subsynoptic and mesoscale features respectively. Both the OSA and the IFA had 6-hourly soundings. The IFA was centered at 2° S, 156° E. The northernmost point of the IFA was the atoll Kapingamarangi (1° N, 154° E).

Radiosondes were launched from air conditioned vans at Nauru and Kapingamarangi. The surface observing stations consisted of a 10 m tower that included a propeller vane wind monitor, pressure, temperature, and humidity sensors. This independently measured surface data was then integrated into the radiosonde data with the first point of the sounding data coming from the surface instrumentation (Miller and Riddle 1994). There were various problems with the surface data and near-surface humidity values at Kapinga and Nauru (Cole, 1993; Loehrer et al. 1995). These included low-level moisture problems resulting from launching the soundings from cool, dry vans as well as inaccurate calculation of the humidity sensor time constant. Because of these problems, little emphasis will be given to surface humidity measurements at Kapinga.

A tipping bucket rain gauge with a resolution of 0.254 mm measured precipitation at Kapinga (and all land based ISS sites). The gauge was located 0.5 m above the ground and roughly seven or eight meters from the 10 m tower (Miller and Riddle 1994). Optical rain gauges measured precipitation for the ship sites (Wang et al. 1979).

The Improved METeorology (IMET) buoy, operated by Dr. Robert Weller and the Woods Hole Oceanographic Institution (WHOI), was located at the IFA center (1° 45' S, 156° E).

It provided surface wind, relative humidity (RH), air temperature, SST, and barometric pressure data at that location (Weller and Anderson 1995). The sea surface temperature was measured at a depth of 0.45 m while the surface latent and sensible heat fluxes were calculated using bulk aerodynamic equations developed by Fairall et al. (1996).

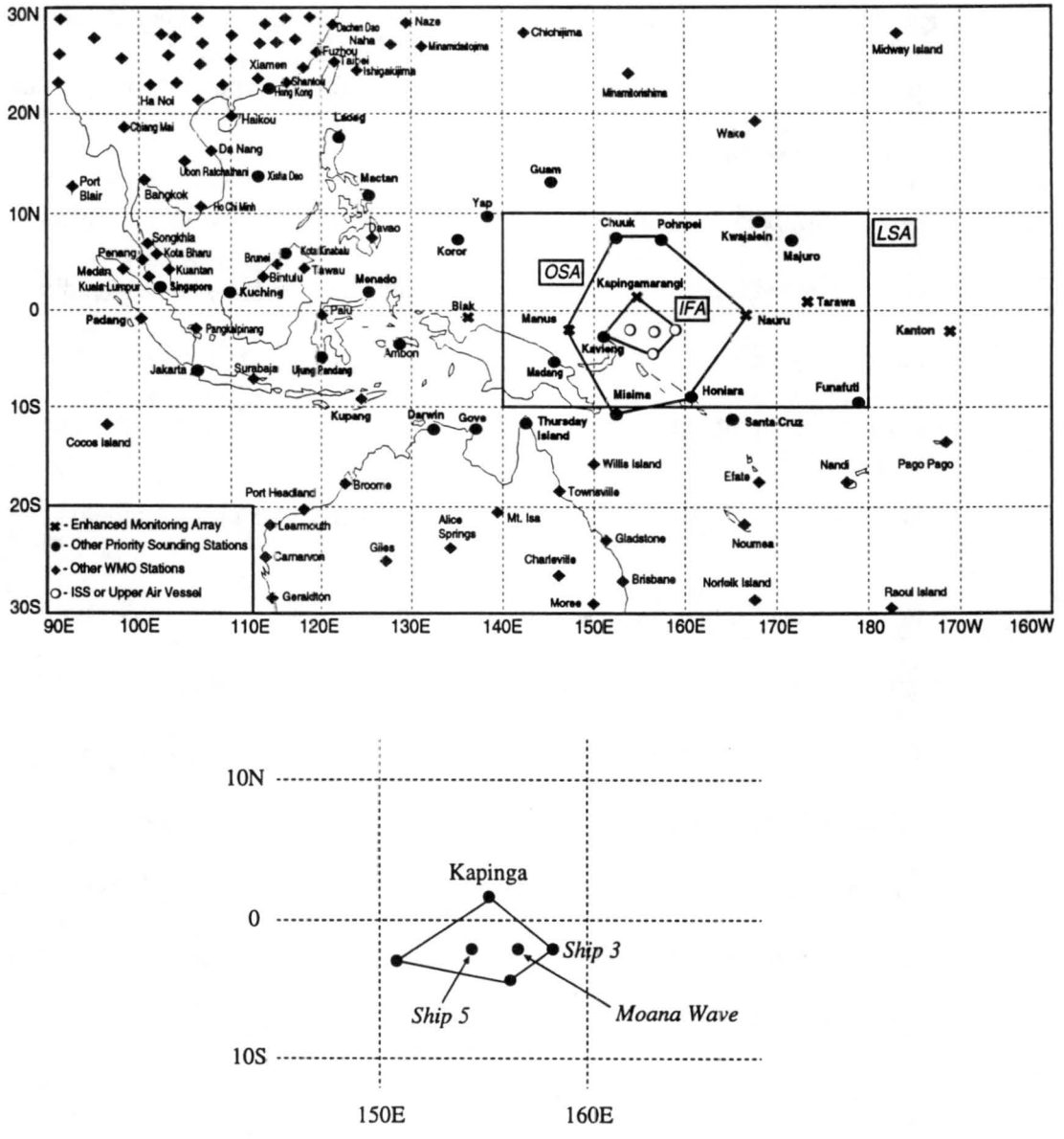

Figure 3.1 The TOGA COARE upper air sounding network. Bottom figure shows a detailed view of the IFA.

3.2 Determination of the Mixed Layer Top

In this study, we used the 6-hourly (4-per-day) soundings from Kapingamarangi (Kapinga for short) to determine mixed layer depths. Kapinga was chosen for the bulk of the analysis for three reasons: 1) it had 6-hourly soundings throughout the 4 month IOP, 2) due to its small size, land effects are minimal (although superadiabatic layers occur, the land influence is less than would be seen at Kaveing), 3) it is close to the center of the IFA where independent measurements have been made of the surface fluxes. This is important since no flux measurements were recorded at Kapinga -- only surface variables.

Well-mixed (vertical) profiles of θ and q capped by ~100-150 m deep entrainment zone identify the mixed layer. We determined the mixed layer top (z_i) of each sounding subjectively by individually locating the entrainment zone marked by a sharp increase in stability (increase in θ) and decrease in moisture (q) (Figure 3.2). Theta profiles in the low-levels must be nearly vertical (i.e., $\frac{\partial \theta}{\partial z} \approx 0$) to qualify as a mixed layer. Although q profiles should also be nearly vertical, they tended to be more erratic. Therefore, we relied slightly more on the θ profiles. In general, the two profiles agreed. At times the specific humidity began to decrease approximately 5 mb before the increase in θ. In these cases, we chose the level corresponding to the θ increase. We discarded stable soundings as well as those that lacked a discernible mixed layer top. The data from the discarded soundings were not used in any of the analyses. Figure 3.3 is an example of a sounding without a detectable mixed layer. Figure 3.4 shows a sounding with a mixed layer that is not as immediately obvious to identify as in Figure 3.2. However, a detectable slope change in the θ profile and a more dramatic drop in specific humidity serve to identify the top. An additional sharp change in stability and moisture is seen near 900 mb. The nature of this

feature is not clear. It is too low to be the trade wind inversion (Johnson et al. 1996), but may be evidence of a dry intrusion (Mapes and Zuidema 1996).

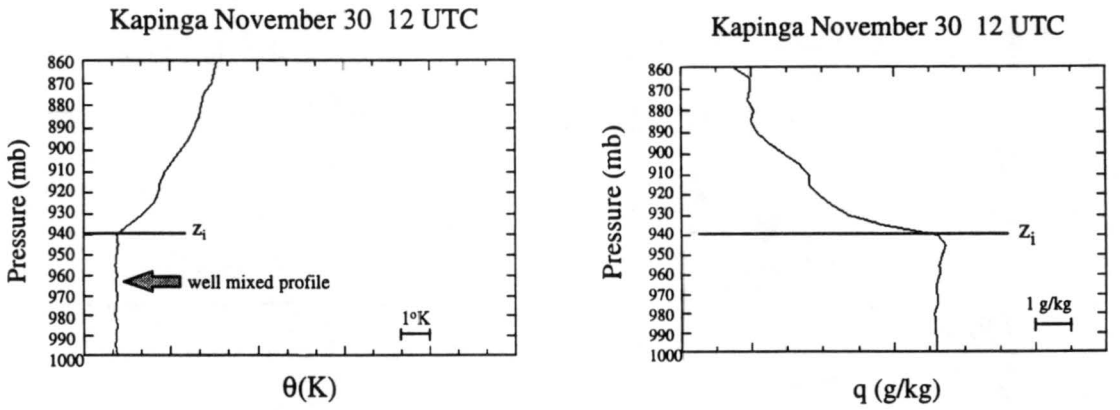

Figure 3.2 Example showing the mixed layer top (z_i) detected by a sharp increase in θ and drop-off in q. Each increment represents 1°K degree or 1 g/kg.

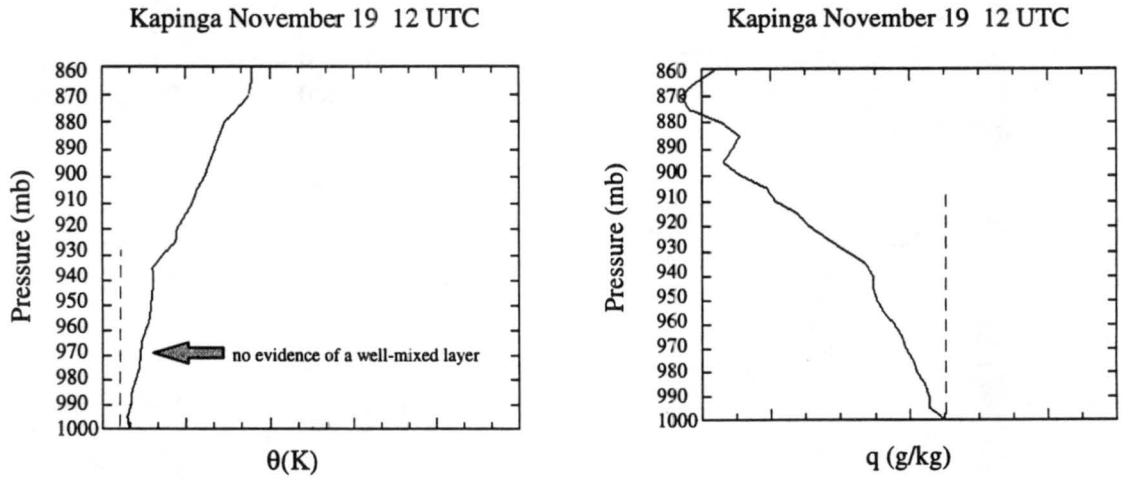

Figure 3.3 Example of a sounding where the mixed layer is not detectable in either the θ or q profile. Each increment represents 1°K degree or 1 g/kg. Dashed lines are provided as a reference of a zero vertical gradient.

As a final example, Figure 3.5 shows a fairly well-mixed θ profile and suggests an entrainment zone between 965 and 945 mb. The q sounding also exhibits a significant decrease at 965 mb; however, below 965 mb, q is not vertical. Instead, it initially shows a small increase and then a small decrease. This is an example of a questionable sounding for determining the well-mixed layer because of the variations in q. We identified the top of the mixed layer by the

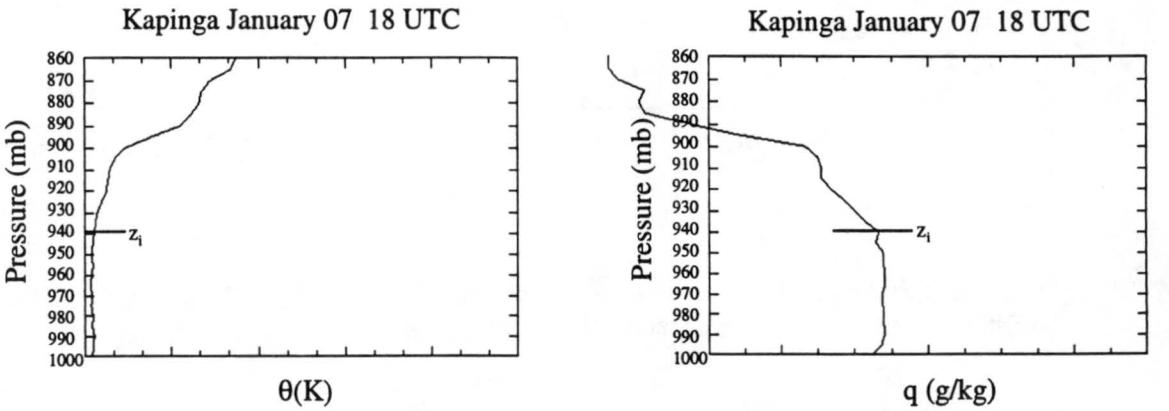

Figure 3.4 The mixed layer is not immediately obvious in the θ sounding; however, a small slope change in θ and comparison with the q profile identifies the top. Each increment represents 1°K degree or 1 g/kg.

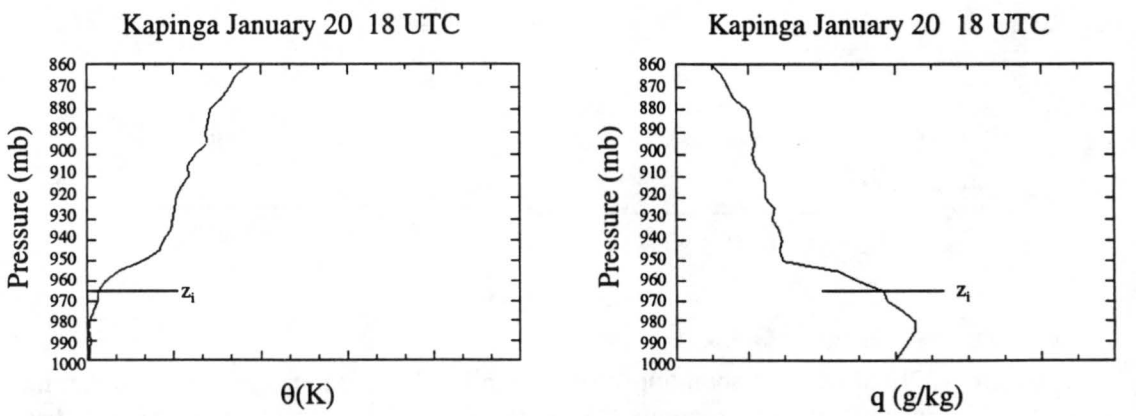

Figure 3.5 An example of a questionable sounding due to variations in q in the mixed layer. This sounding was included in the analysis due to the fairly well-mixed θ profile and the significant increase in θ and decrease in q at 965 mb. Each increment represents 1°K degree or 1 g/kg.

significant changes in both the θ and q soundings at 965 mb along with the fairly well-mixed θ profile below 965 mb. Had θ been less well-mixed we would have discarded this sounding. Note that the q variations were ± 0.3 g/kg and the θ profile decreased 0.2°K near the top of the mixed layer. Such variations are not significant because they are within the accuracy of the sonde (Miller and Riddle 1994).

Using this subjective method, 75% (356 out of 475) of the soundings at Kapinga revealed detectable mixed layers. This is consistent with Fitzjarrald and Garstang (1981) who used the Boundary Layer Instrumentation System (BLIS) and data from the GARP Atlantic Tropical Experiment (GATE) to objectively determine mixed layer tops by fitting each profile with a slightly smoothed cubic spline. Of the total 703 GATE profiles, 559 (79.5%) showed a mixed layer structure using this objective method (Fitzjarrald and Garstang 1981).

An analysis at a single station is insightful, but it may not be representative of the entire region. Therefore, in addition to Kapinga, we analyzed mixed layer tops from soundings on three research vessels: *Shyian 3* (hereafter referred to as *Ship 3*), *Xiangyanghong 5* (hereafter referred to as *Ship 5*), and the *Moana Wave*. The cruise dates for these ships are listed in Table 3.1. Together, these four stations cover a large portion of the IFA (Figure 3.1).

	Cruise 1	***Cruise 2***	***Cruise 3***
Ship 3	Nov 10 - Dec 12	Dec 18 - Jan 23	Jan 31 - Feb 18
Ship 5	Nov 05 - Nov 20*	Dec 04 - Jan 09	Jan 24 - Feb 19
Moana Wave	Nov 11 - Dec 03	Dec 18 - Jan 02	Jan 28 - Feb 14

Table 3.1 Cruise dates for the three ship sites used in this study. *There were no high resolution sounding data available for cruise 1 of *Ship 5*. Therefore, analysis for *Ship 5* was performed for only cruises 2 and 3.

Chapter 4

PROCESSES CONTROLLING THE MIXED LAYER DEPTH

4.1 Undisturbed Conditions

In this section we adopt a simple, one-dimensional mixed layer model (Tennekes 1973) to illustrate how the mixed layer responds to its environment in undisturbed conditions. The model assumes the entrainment zone, which is typically 100-200 m deep, is reduced to an infinitesimal depth in order to achieve zero-order jumps in potential temperature and heat flux at the top of the mixed layer (Figure 4.1).

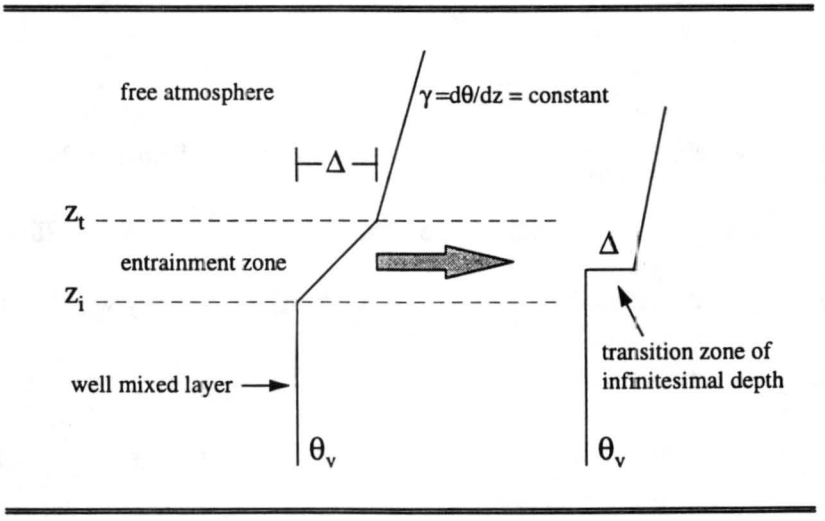

Figure 4.1 Schematic diagram of the tropical boundary layer θ_v profile. The inversion strength is indicated by Δ.

The inversion strength (Δ) is defined by the virtual potential temperature difference at the top and the bottom of the entrainment zone $\left(\overline{\theta}_v(z_t)-\overline{\theta}_v(z_i)\right)$. The buoyancy flux, $F\equiv\left(\overline{w'\theta_v'}\right)$, is given by the equation:

$$F=E\left(B+0.61\left(\frac{c_p}{L_v}\right)\overline{T}\right) \tag{4.1}$$

where E is the latent heat flux, B is the Bowen ratio (i.e., the sensible heat flux divided by the latent heat flux), c_p is the specific heat, L_v is the latent heat of evaporation, T is the temperature and the overbar denotes a mean value. It is shown in Tennekes (1973) that the change in the mixed layer depth is given by:

$$\frac{\partial z_i}{\partial t}=\overline{w}_i-\frac{F_i}{\Delta} \tag{4.2}$$

where $\overline{w}_i$ is the mean vertical velocity and the subscript i denotes values at z_i. This says that the mixed layer depth is proportional to the vertical motion and buoyancy flux at z_i and inversely proportional to the strength of the inversion. Therefore, the only way the mixed layer can grow in a subsiding environment (negative $\overline{w}_i$) is if $F_i < 0$ indicating a negative heat flux at the inversion. Thus, the mixed layer depth increases as the surface sensible and latent heat fluxes increase (causing F to increase). Finally, a weak inversion (Δ) allows the mixed layer to grow. As the strength of the inversion approaches zero, the mixed layer grows rapidly. Tennekes (1973) derives another equation for Δ which, when coupled with (4.2), can be solved for z_i and Δ assuming F_i and $\overline{w}_i$ are known. F_i is often parameterized as a function of the surface buoyancy

flux (i.e., $F_i = -kF_s$, where F_s is the surface value and k is a positive constant, Tennekes 1973). However, $\overline{w}_i$ is very difficult to determine accurately, which limits our ability to solve the coupled system for z_i and Δ.

To determine an equation for the change in the mixed layer mean virtual potential temperature $\left(\overline{\theta}_v\right)$ with time, note that for adiabatic conditions (i.e., $\frac{D\theta_v}{Dt}=0$) :

$$\frac{\partial\overline{\theta}_v}{\partial t} + \nabla_H \cdot \overline{v}\,\overline{\theta}_v + \frac{\partial\overline{w\theta}_v}{\partial z} = -\frac{\partial\left(\overline{w'\theta_v'}\right)}{\partial z} \tag{4.3}$$

which can be written:

$$\frac{\partial\overline{\theta}_v}{\partial t} + \overline{v}\cdot\nabla_H\overline{\theta}_v + \overline{w}\frac{\partial\overline{\theta}_v}{\partial z} = -\frac{\partial\left(\overline{w'\theta_v'}\right)}{\partial z}. \tag{4.4}$$

In a well-mixed layer $\nabla_H\overline{\theta}_v = \frac{\partial\overline{\theta}_v}{\partial z} = 0$, therefore:

$$\frac{\partial\,\overline{\theta}_v}{\partial\,t} = -\frac{\partial\left(\overline{w'\theta_v'}\right)}{\partial z} \tag{4.5}$$

This says that the change in the mean virtual potential temperature in the mixed layer with time is equal to the negative of the change in the buoyancy flux with height. (4.5) can be integrated from $z = z_s$ to $z = z_i$ (where z_s is the top of the surface layer) to get:

$$\frac{\partial\overline{\theta}_v}{\partial t} = \frac{F_s - F_i}{z_i} \tag{4.6}$$

This says that the change in the mean virtual potential temperature of the mixed layer with time is equal to the difference between the buoyancy flux at the top of the surface layer and the heat flux at the top of the mixed layer divided by the mixed layer depth. Under typical circumstances, $F_s \neq F_i$ and it is impossible to achieve a steady-state solution using (4.6). In order to offset the flux convergence of heat by the eddies, we must include a radiative cooling term in (4.3) such that (4.6) becomes:

$$\frac{\partial \overline{\theta}_v}{\partial t} = \frac{F_s - F_i}{z_i} + Q_{Rm} \tag{4.7}$$

where Q_{Rm} is the vertically integrated radiative heating rate. Setting $\frac{\partial \overline{\theta}_v}{\partial t} = 0$, we can solve for z_i under steady-state conditions:

$$z_i = -\frac{F_s - F_i}{Q_{Rm}} \tag{4.8}$$

or using the closure $F_i = -kF_s$ for free convection (Stull 1993), where k is a positive constant:

$$z_i = -\frac{(1+k)F_s}{Q_{Rm}} \tag{4.9}$$

For periods of steady mixed layer depth, (4.9) can be used to determine z_i if F_s and Q_{Rm} are known. On the other hand, (4.7) can be used for undisturbed situations where there is a diurnal cycle in the mixed layer depth to solve for Q_{Rm} as a residual. This approach will be used in this thesis and comparisons made with independent radiative heating estimates.

4.2 Disturbed Conditions

The mixed layer is substantially modified, if not destroyed, in the presence of convection. Warm sea surface temperatures in the equatorial western Pacific ignite strong and frequent convection that often takes the form of mesoscale convective systems (MCSs). MCSs consist of both convective and stratiform precipitation elements (Houze 1977; Zipser 1977). Convective precipitation is found in the large cumulonimbus towers while the stratiform precipitation is associated with the anvil region. Mid-level downdrafts and subsidence warming are connected to the low-intensity stratiform precipitation (Zipser 1977). These downdrafts are weak and seldom reach the sea surface. Convective rain, on the other hand, produces intense, short-lived downdrafts. These rain-driven downdrafts force mid-level air down to the sea surface where it spreads out to form a convective wake (Zipser 1977; Fitzjarrald and Garstang 1981; Johnson and Nicholls 1983). The convective wake modifies the existing boundary layer bringing cooler, drier (in an absolute sense), and windier conditions. This results in an increase in the surface fluxes of latent and sensible heat. With time, the boundary layer recovers to its preconvective conditions.

4.2.1 Criteria

Young and Perugini (1995) determined specific criteria to mark the beginning and end of a convective wake. By their definition, a convective wake begins when a rain-driven downdraft reaches the surface and ends when the boundary layer temperature is no longer dominated by wake-recovery processes. They used a precipitation rate of at least 2 mm/hr to define the beginning of a convective wake. They based this precipitation rate criteria upon the results of Barnes and Garstang (1982) during GATE. Barnes and Garstang (1982) found rainfall rates of 2 mm/hr were necessary to produce downdrafts capable of inducing changes in the temperature and humidity in the surface layer. When this threshold is exceeded, the total moist static energy in

the subcloud layer decreases, implying the downward transport of cooler and drier air from below the mid-tropospheric minimum in total static energy (Fitzjarrald and Garstang 1981). For rainfall rates less than 2 mm/hr, evaporation of rainwater within the subcloud layer dominates temperature and humidity changes (Barnes and Garstang 1982).

To determine when the wake-recovery process has ended, Young and Perugini (1995) outlined two possible criteria: 1) When the difference between the SST and the air temperature (SST - air temperature) is equal to zero or becomes negative. This marks a return to equilibrium between the boundary layer and sea surface temperature. 2) The first hour for which the 5 hour running mean air temperature decreases, thus ending the warming recovery. This indicates that other processes, such as advection, have become the dominating mechanism in the boundary layer temperature budget.

4.2.2 Example of a Convective Wake

A convective wake occurred during the TOGA COARE IOP on February 10, 1993. The data in this example were collected at the IMET buoy located at 1° 45'S, 156° E. Radar data for February 10 shows a line of convection followed by a large area consisting of stratiform precipitation and embedded convective cells (Figure 4.2). At 0230 UTC (1230L) the IMET buoy, represented by the top asterisk, is in the convective rain region. The intense downdrafts from this precipitation produced a convective wake that modified the boundary layer. By 0300 UTC (1300L), the leading line of convection had moved west of the IMET buoy. By this time, the boundary layer was in the process of recovering to its pre-convective conditions.

a. Precipitation

The typical precipitation pattern associated with the passage of a MCS is a sharp peak representing convection followed by a secondary maximum for the stratiform rain and a

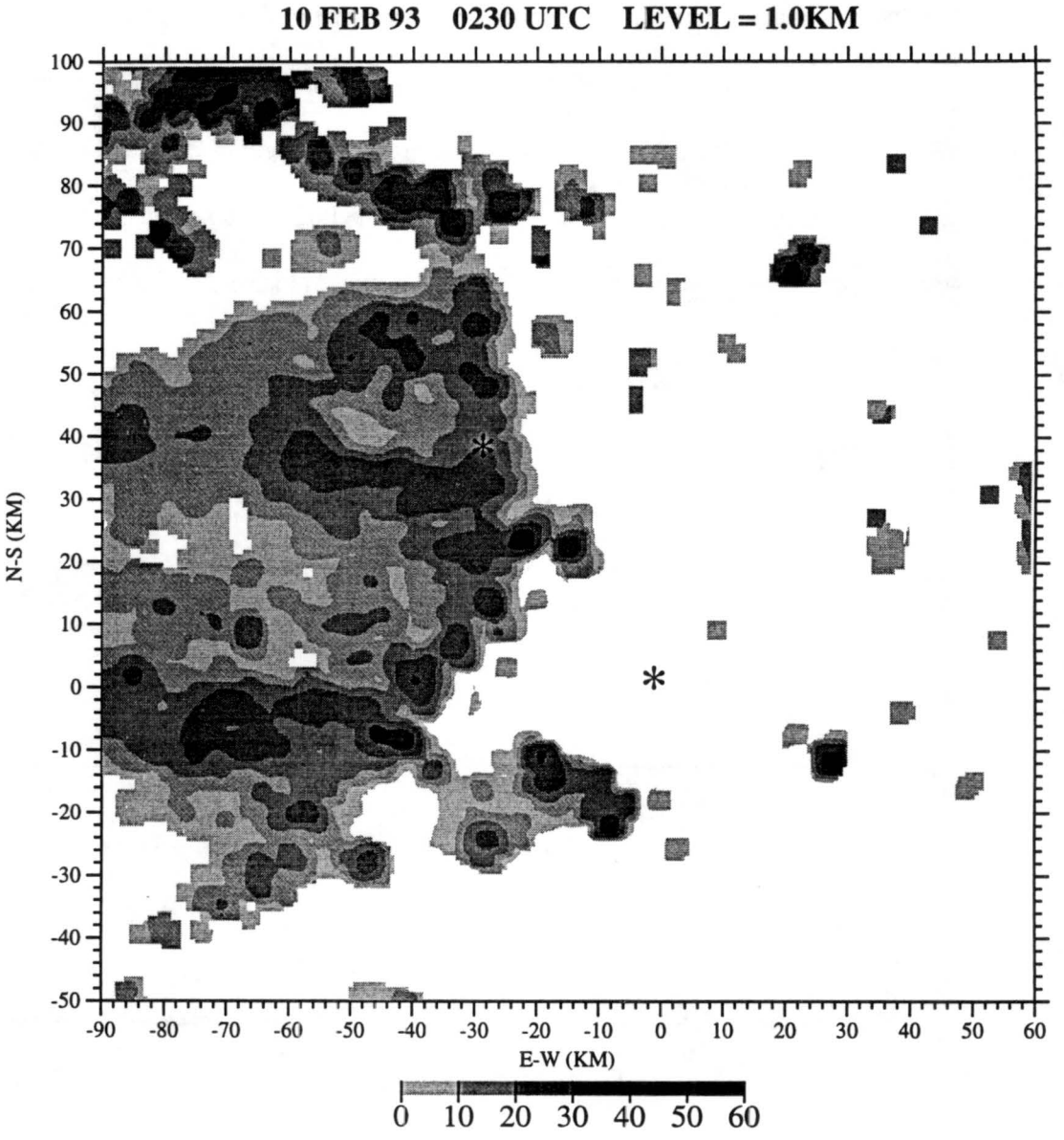

Figure 4.2 Radar image of the squall line that passed over the IMET buoy on February 10, 1993 at 0230 UTC. The IMET buoy is denoted by the top asterisk. Image courtesy of Tom Saxon.

minimum between the two (e.g., Johnson and Hamilton 1988). The gap between the rainfall peaks is due to subsidence behind the leading convective cells and the rearward transport of snow and ice in the system-relative front-to-rear flow aloft (Smull and Houze 1985; Rutledge and Houze 1987). As mentioned earlier, the convective wake is associated with the convective rain, although is spreads out over an area much larger than that of the convective cells.

Figure 4.3 shows the rainfall rate in the vicinity of the IMET buoy as derived from radar reflectivities (Rickenbach 1995). The calculation is for a height of 2 km and averages the rainfall rate volumetrically in a 1 km x 1 km region around the IMET buoy. Thus, if the rainfall rate were measured just at the point where the IMET buoy was located, the rates would be much higher.

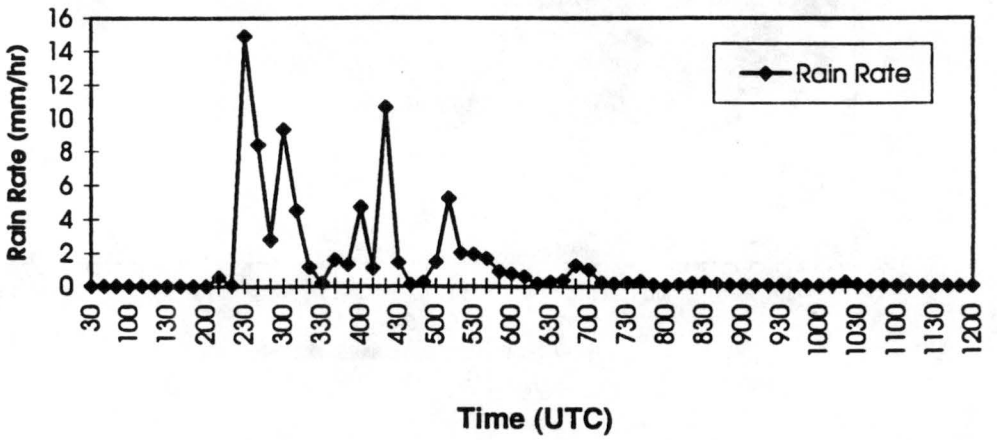

Figure 4.3 Rain rate derived from radar reflectivities in a 1 km x 1 km area in the vicinity of the IMET buoy. Figure by Tom Saxon using the algorithm created by Tom Rickenbach.

Rickenbach (1995) used empirical relations to translate reflectivity into an actual rainfall rate (personal communication, 1996). However, different relations apply to convective and stratiform precipitation. Therefore, each echo was first denoted as one type or the other. In Figure 4.3, the peak at 0230 UTC corresponds to the onset of convective precipitation. Although the system also contained elements of stratiform rain, the small peaks do not necessarily represent stratiform precipitation but may be embedded convective cells behind the leading squall line. Nevertheless, the initial convective rain is what formed the downdrafts that then modified the boundary layer.

b. Temperature

With the onset of convection at the IMET buoy, the temperature dropped 4.4°C from 28.9°C at 0000 UTC to 24.5°C at 0200 UTC (Figure 4.4). This temperature drop is consistent with the findings of Johnson and Nicholls (1983), Young and Perugini (1995), and Parsons et al. (1994). Although the boundary layer cooled very rapidly, it took approximately 10 hours for it to recover to its pre-convective temperature of 28.9°C (reached at 1200 UTC).

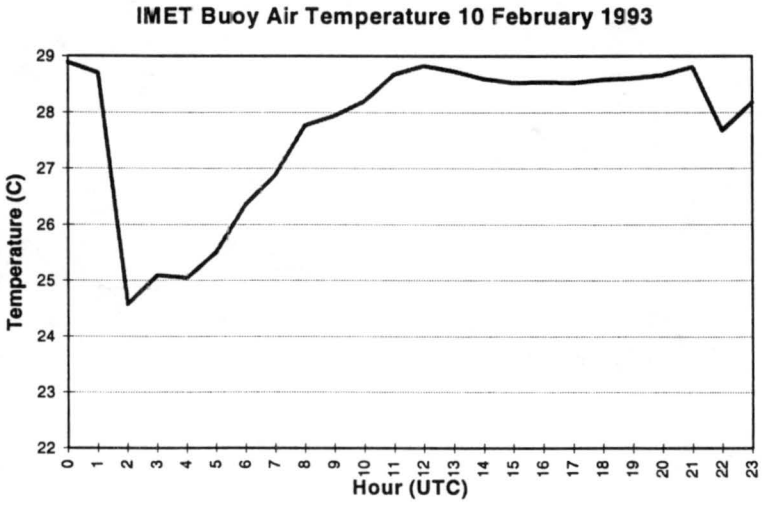

Figure 4.4. The large drop in the air temperature at 0200 UTC indicates the passage of the wake at the IMET buoy on 10 February 1993.

c. Wind

Beside the drop in boundary layer temperature, the convective wake is visible in the wind data (Figure 4.5). As the rain-driven downdraft hits the ocean surface and spreads out, the winds increase. Figure 4.5 shows a sharp peak in the total wind at 0200 UTC.

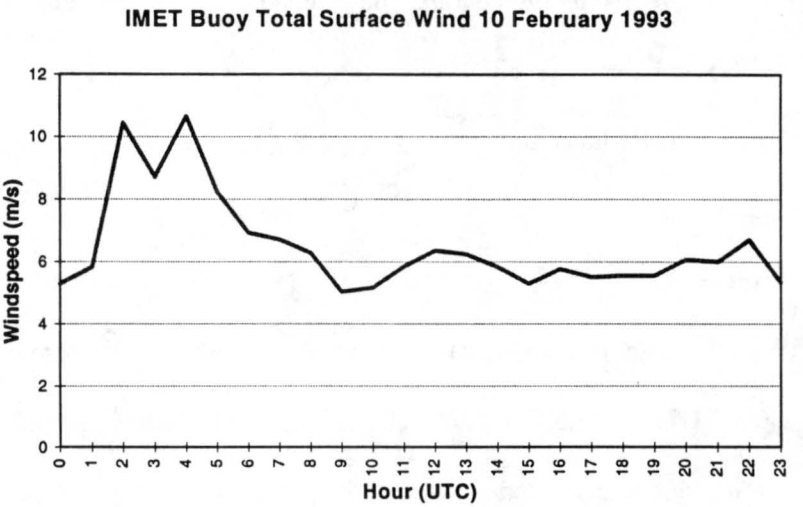

Figure 4.5 Surface wind increases behind the leading convection. Measured at the IMET buoy 10 February 1993.

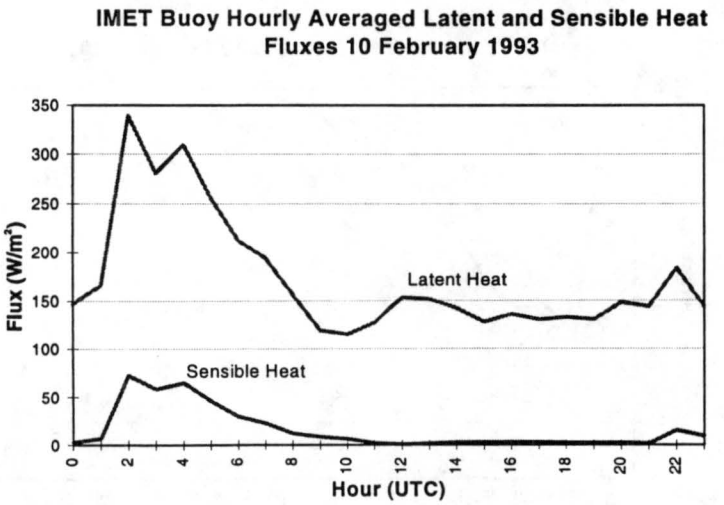

Figure 4.6 Surface heat fluxes at the IMET buoy during the passage of the convective wake on 10 February 1993.

d. Surface Fluxes

The combination of increased surface winds and reduced air temperatures causes an increase in both the latent and sensible heat fluxes. As expected, both fluxes exhibit a sharp increase at 0200 UTC (Figure 4.6).

e. Specific Humidity

Finally, the descending mid-level air dries the boundary layer thus reducing the specific humidity (q) in the wake region (Figure 4.7). As shown by Johnson and Nicholls (1983), the maximum depression in q often occurs 3 to 4 hours after the squall passage. This lag is not evident in the data taken at the IMET buoy for the February 10 event; however, greater spatial resolution may reveal more information.

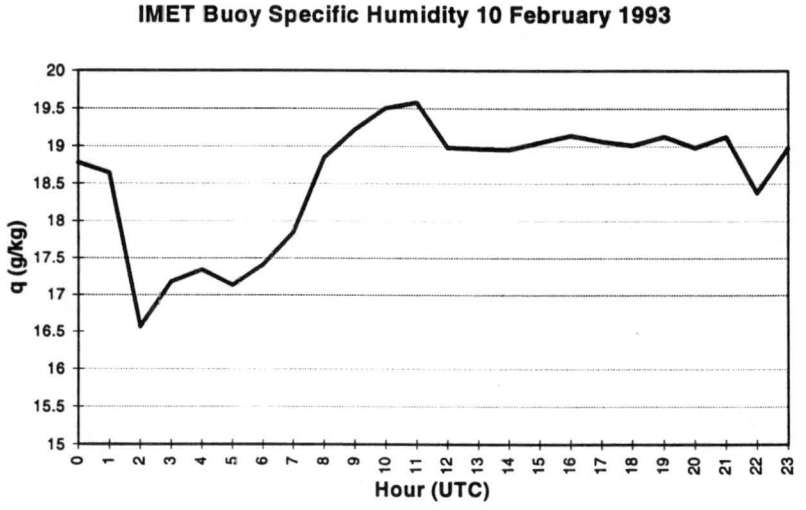

Figure 4.7 The specific humidity drops as the dry, mid-level air penetrates the boundary layer. Measured at the IMET buoy on 10 February 1993.

4.2.3 Recovery

The cooler, drier, boundary layer returns to its pre-convective state 2 to 10 hours after the onset of the convective wake. The already cool, stable boundary layer is often capped by warm downdrafts in the lower troposphere associated with the anvil region of the MCS. This subsidence delays the growth of the mixed layer and slows boundary layer recovery (Young and Perugini 1995; Zipser 1977). The temperature recovery begins quickly but then slows as the air-sea temperature difference decreases and reduces the sensible heat flux to the atmosphere.

Later in this study, we will analyze the buoyancy flux at the IMET buoy and compare it to the mixed layer top at Kapinga. Precipitation events caused convective wakes to be an important factor in analyzing the mean properties of the mixed layer. The convective wake signature appears in the analyses of numerous mixed layer variables. Oftentimes, we analyze the mixed layer during a specified light-wind period in an effort to reduce the effects of convective wakes.

Chapter 5

LONG-TERM VARIABILITY

5.1 Mixed Layer Depth

Figure 5.1 shows the time series of the detectable mixed layer tops at Kapinga during the IOP. Lines connect times when there were consecutive mixed layers. The figure shows a low-frequency oscillation as the mixed layer grows and shrinks over the four-month period. This suggests that the mixed layer depth is modulated by the 40-50 day oscillation (Madden and Julian 1972).

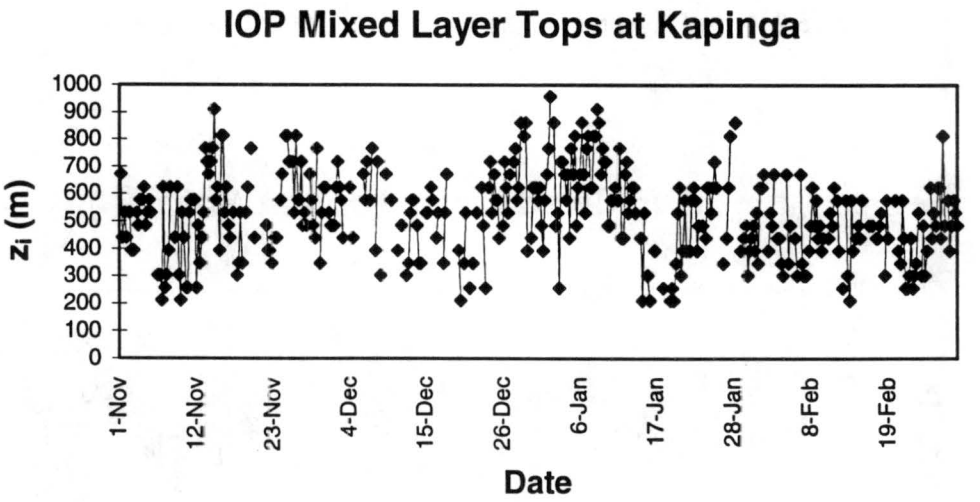

Figure 5.1 Mixed layer tops at Kapinga for the IOP. Consecutive sounding data are connected while gaps indicate times where no mixed layer was detectable.

Since the ship data sets are broken up into cruises, the long-term variability of the mixed layer top is less obvious. However, certain features of the same oscillation in z_i at Kapinga are

also apparent for the ships (Figures 5.2 - 5.4). Note the times when the mixed layer is deep at all four sites (i.e., the middle of November and the end of December).

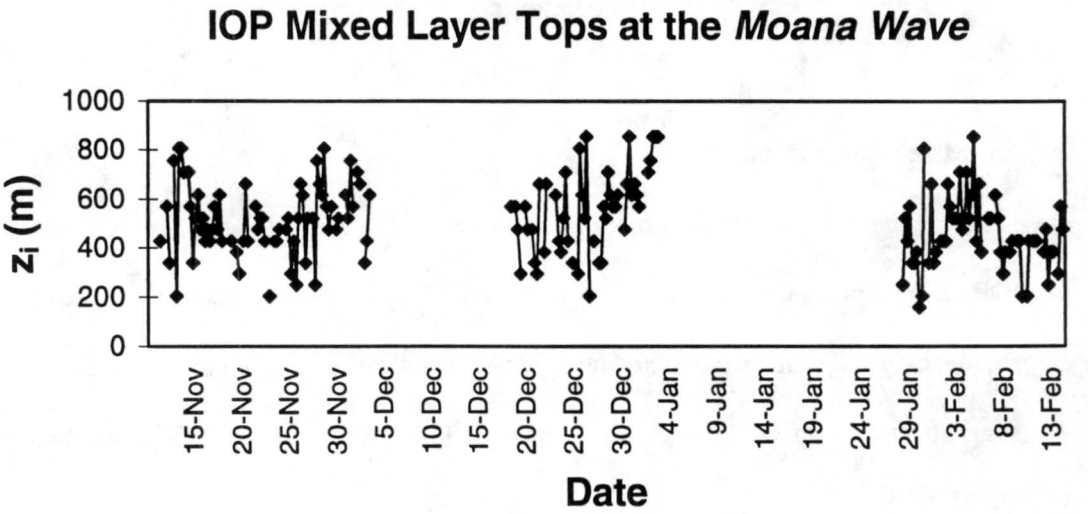

Figure 5.2 Mixed layer tops at the *Moana Wave* for all three cruises.

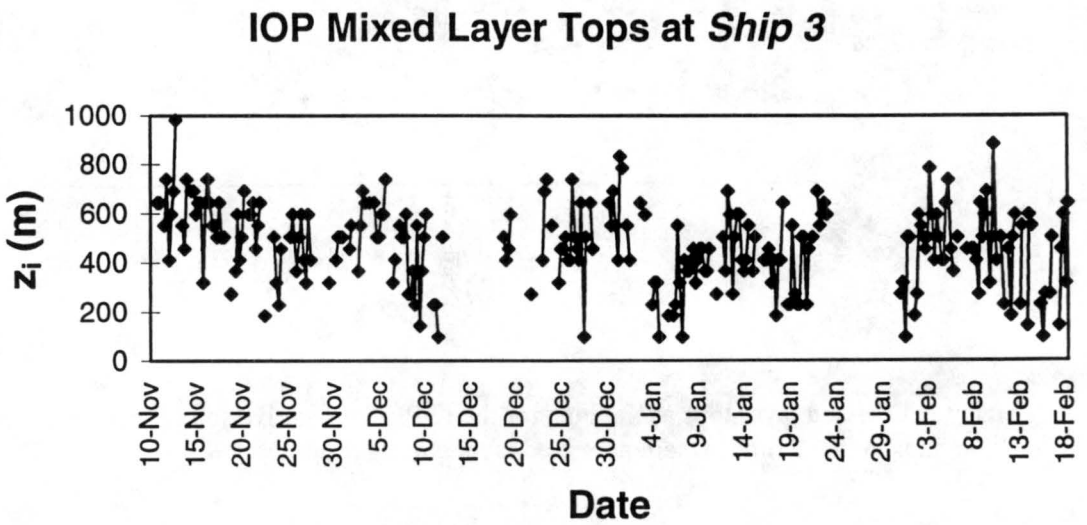

Figure 5.3 Mixed layer tops at *Ship 3* for all three cruises

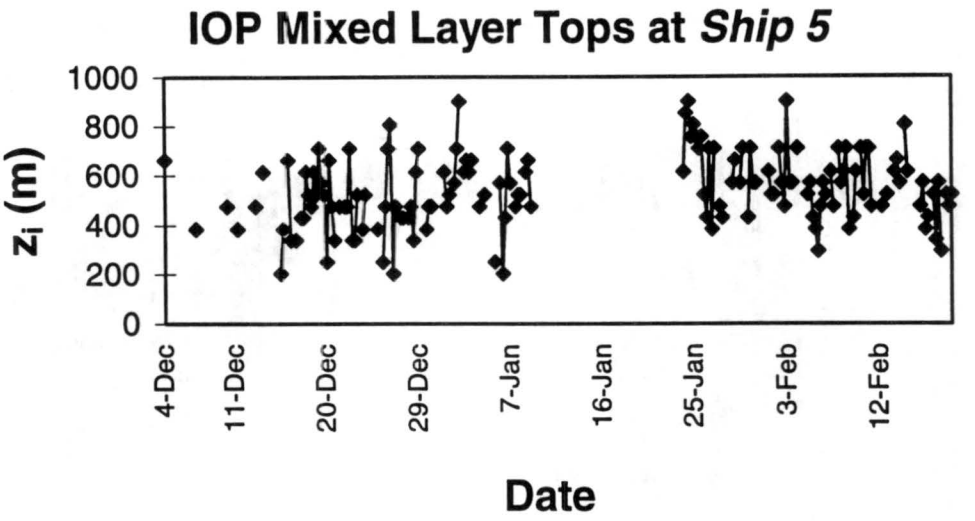

Figure 5.4 Mixed layer tops at *Ship 5* for cruises 2 and 3.

In Chapter 4 we presented an equation for the buoyancy flux and related this flux to the mixed layer depth. Figure 5.5 shows a time series of the mixed layer tops at Kapinga and the buoyancy flux at the IMET buoy. The buoyancy flux can only be calculated at the IMET buoy where surface flux data is available; however, the proximity of the two locations validates a general comparison. Figure 5.5 seems to contradict (4.2) that says that the change in the mixed layer top with time is directly proportional to the buoyancy flux at the mixed layer top (which, as discussed earlier, is related to the surface buoyancy flux). Specifically, the figure shows that oftentimes when the buoyancy flux was large, the mixed layer tops were low. However, as will be seen later, times when the buoyancy flux was large often corresponded to periods of rainfall. Since the simple mixed layer model only applies to undisturbed conditions, we can conclude that this model does not work much of the time in TOGA COARE. Nevertheless, if applied selectively to non-precipitating periods, it can yield some insight into the mixed layer dynamics.

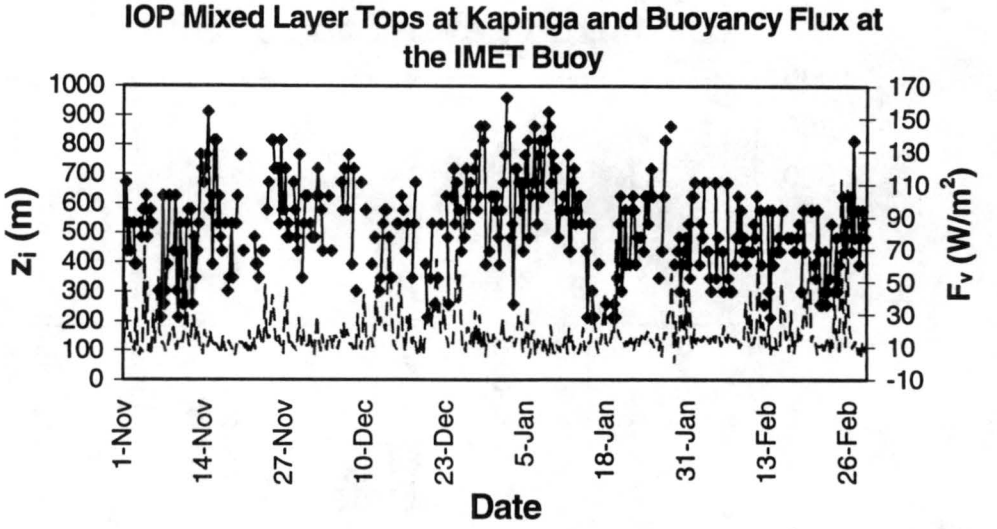

Figure 5.5 Mixed layer tops (diamonds) at Kapinga and buoyancy flux at the IMET buoy (dashed gray line) for the IOP.

5.2 Effects of Convection

Due to the frequency of precipitation events in this region, a study of the mixed layer must include the impacts of convection. In general, the height of the cloud base is found at approximately the top of the entrainment zone (~100 m above the top of the mixed layer) (e.g., Deardorff 1975, and others). However, the top of the entrainment zone was not always detectable in the TOGA COARE sounding data. Thus, it is useful to compute the lifting condensation level (LCL) of the mixed layer air to get an idea of the variability of cloud-base height.

We calculated the lifting condensation levels (LCLs) at each station by first computing the air temperature at the LCL using the equation found in Bolton (1980):

$$T_{LCL}(K) = \frac{2840}{\left[3.5Ln(T_k) - Ln(e) - 4.805\right]} + 55 \qquad (5.1)$$

where T_k is the air temperature in degrees Kelvin and e is the vapor pressure. Due to the questionable surface values at Kapinga, we used the mean q and mean θ in the mixed layer to calculate the LCL temperature. The mean value of q was drier than the surface value and which led to higher LCLs. Note, to test this method, we also calculated the LCL at Kapinga using the surface values. However, this produced unreasonably low LCLs (the average LCL using this method was 527.6 m -- approximately 12 m above the average z_i at Kapinga) due to the higher surface moisture values.

The mean θ value was brought down to the surface using Poisson's equation:

$$\overline{\theta} = T_k \left(\frac{1000}{p} \right)^{\frac{R}{cp}} \tag{5.2}$$

After finding the temperature at the LCL, we calculated the height of the LCL using the dry adiabatic lapse rate of 9.8°K/km. The lapse rate is equal to the difference between the surface temperature and the temperature at the LCL divided by the height, Z (Figure 5.6).

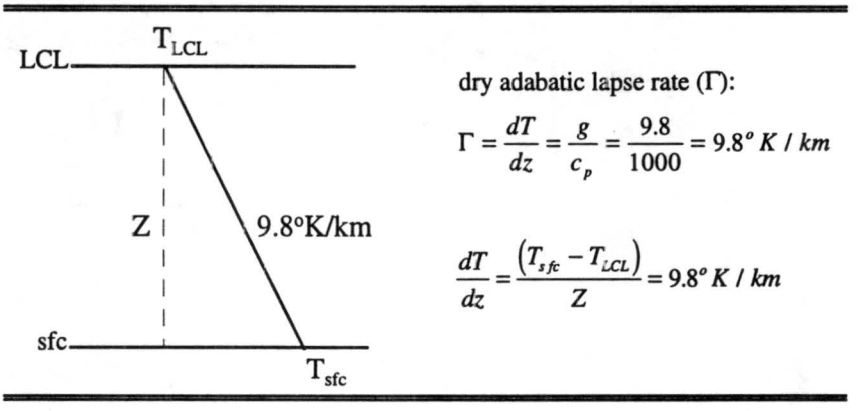

Figure 5.6 Schematic illustrating the geometry of the lapse rate up to the LCL and the equations governing this relationship.

Therefore, the LCL height is given by:

$$z_{LCL} = \frac{T_{sfc} - T_{LCL}}{9.8} \tag{5.3}$$

Fitzjarrald and Garstang (1981) found the mean cloud base, defined by the average LCL of the mixed layer air, to be 652 m. Furthermore, they found the mean entrainment zone top to be 607 m, roughly 50 m below the average LCL. With an average entrainment zone depth of 100 m, we can assume the LCL should be approximately 150 m above the mixed layer top. Figure 5.7 shows the IOP time series of LCLs at Kapinga. Frequently, the LCLs were indeed 150-200 m above the mixed layer top; however, during clear conditions they were substantially higher than z_i. The mean LCL at Kapinga was 838 m, 323 m higher than the mean z_i.

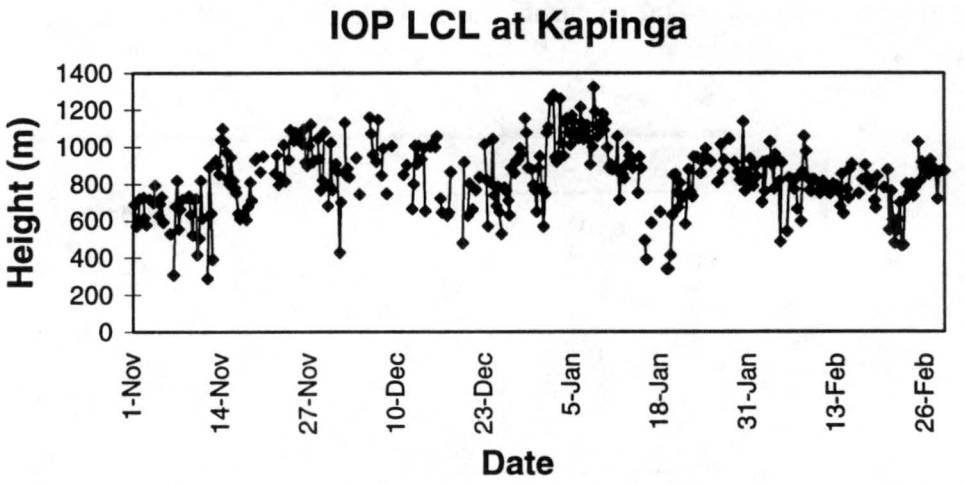

Figure 5.7 IOP time series of the lifting condensation levels (LCLs) at Kapinga. LCLs were calculated using the mean q and mean θ in the mixed layer.

A time series comparison of the mixed layer tops and LCLs (Figure 5.8) gives some indication of when the mixed layer was disturbed by convection and when clouds could be found near the mixed layer top (e.g., z_i and the LCL were in close proximity at the beginning of November and the end of December). When the LCL was markedly above z_i, only widely scattered clouds formed atop the mixed layer (e.g., the beginning of January).

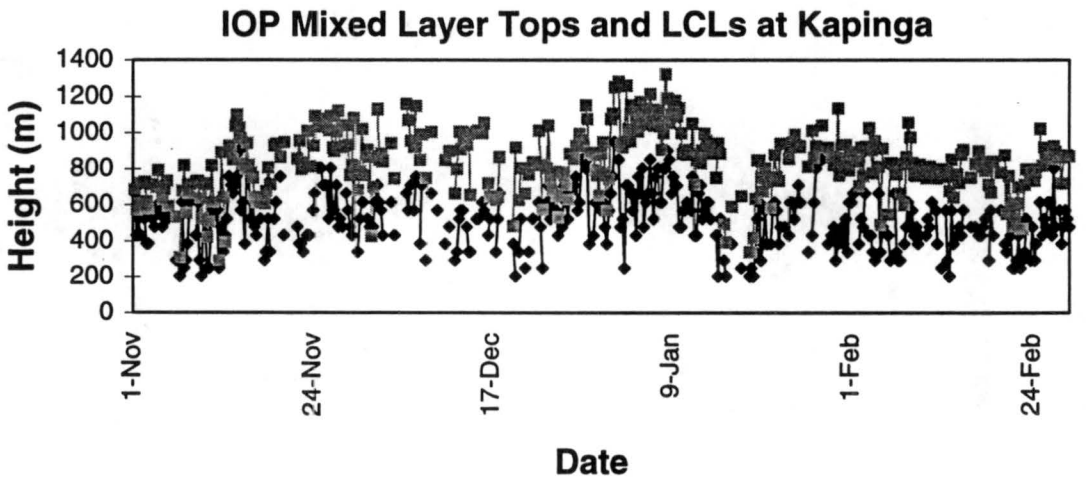

Figure 5.8 Time series of mixed layer tops (diamonds) and LCLs (squares) at Kapinga for the IOP.

As an additional source of data, a laser ceilometer aboard the *Moana Wave* measured cloud base height (White and Fairall 1996). Mapes and Zuidema (personal communication, 1996) used this ceilometer data (made available by Dr. Allen White) and plotted the cloud base height for all the times the *Moana Wave* was at sea (Figure 5.9). They looked at the lowest 20th percentile of the data in order to isolate cloud base and reduce the cases where the ceilometer was recording the sides of clouds or mid-level debris.

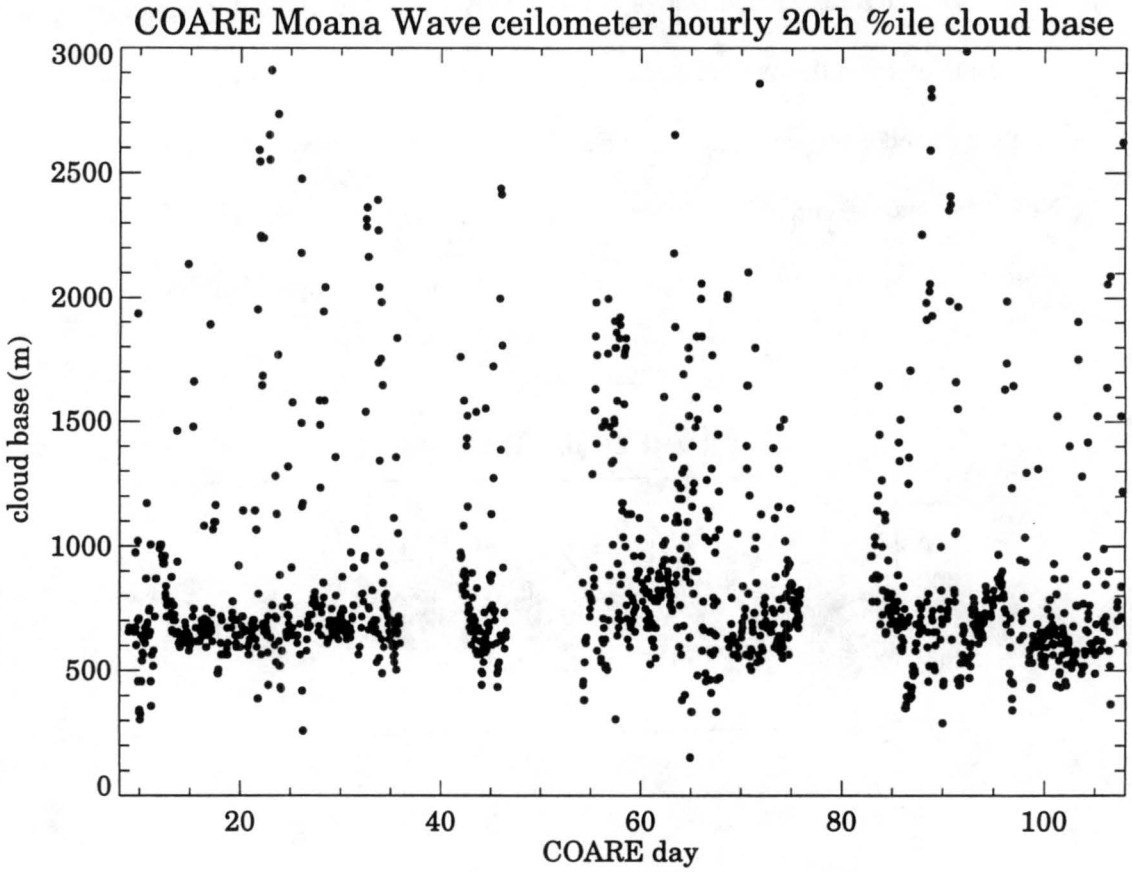

Figure 5.9 20th percentile cloud base heights measured by the laser ceilometer on the *Moana Wave*. (data courtesy of Dr. Allen White).

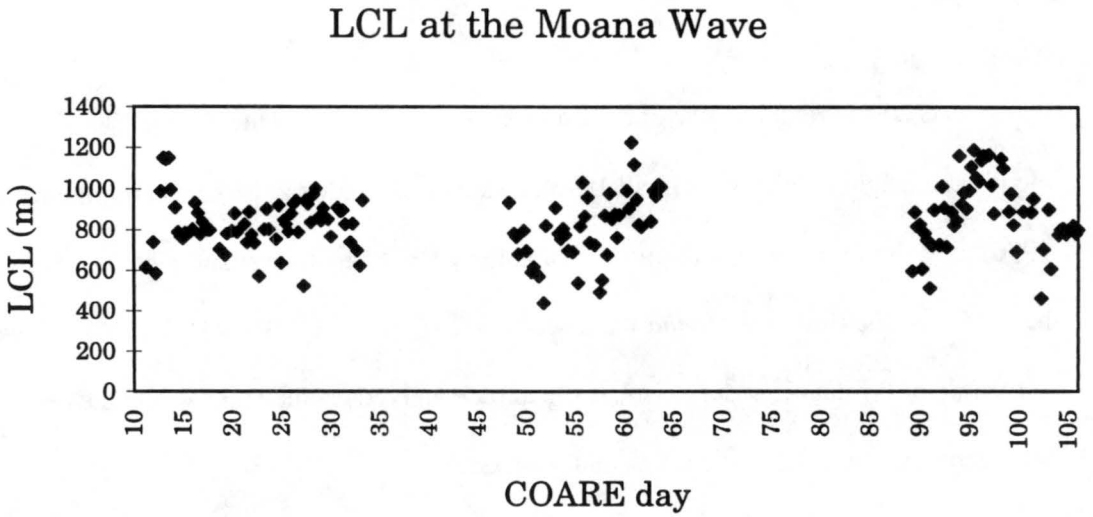

Figure 5.10 LCLs at the *Moana Wave* for all three cruises.

The ceilometer time series is in general agreement with the broken LCL time series at the *Moana Wave*; however, the ceilometer cloud base data is somewhat lower than the LCL heights (Figure 5.10). The ceilometer plot shows a section of data between cruises 1 and 2 of the *Moana Wave* (near day 45). This was recorded as the *Moana Wave* traveled to and from Guam; however, no sounding data were take during this short excursion. Ignoring the additional ceilometer data, the overall trends in both figures are the same for each cruise. This suggests that the cloud base generally follows the LCL.

White and Fairall (1996) also looked at the cloud base at the *Moana Wave* using ceilometer data. They plotted the frequency distribution of cloud bases and found the peak to be at approximately 750 m (Figure 5.11). White and Fairall (1996) calculated a quantity they called ΔZ defined to be the height of the cloud base minus the LCL ($\Delta Z = Z_b$ - LCL). Using surface values to calculate the LCL, the peak in ΔZ turned out to be approximately 150 m. With this difference, and assuming the average cloud base was, in fact, 750 m, the average LCL was located at 600 m. We calculated the mean LCL at the *Moana Wave* to be 839.3 m, substantially higher than White and Fairall (1996). However, the surface values tended to be more moist than the mean mixed layer values. This would lead to substantially lower LCLs.

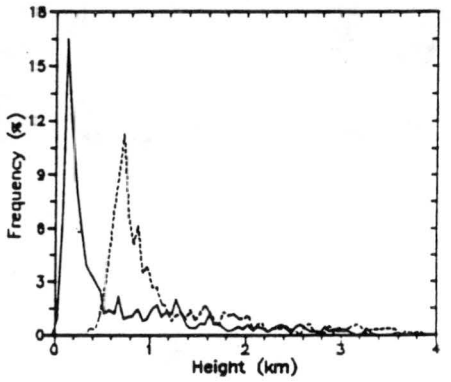

Figure 5.11 The frequency distribution of cloud base (dashed) at the *Moana Wave* (measured by the laser ceilometer) and ΔZ (solid). The LCL used to calculate ΔZ was estimated from near surface measurements of temperature and humidity. From White and Fairall (1996).

To see how vulnerable the LCL at the *Moana Wave* is to changes in moisture, we added 1 g/kg to the mixed layer mean q used in the original calculation[1]. Using these slightly moister values of q, we calculated the mean LCL to be 718.6 m (120.7 m lower than that calculated using only the mixed layer mean q). These lower LCLs would match the cloud base heights measured by the ceilometer better than the original calculation. Note that the mixed layer mean θ was still used in the second calculation. Warmer surface temperatures would also reduce the level of the LCL.

The impact of convection on the mixed layer is also illustrated in Figure 5.12 which shows the time series of z_i and precipitation at Kapinga. Note that the times where the mixed layer was frequently disrupted or shallow often corresponded to precipitation events. During these periods, the boundary layer was either stable or characterized by shallow, recovering convective wakes. Conversely, when the mixed layer was the deepest (i.e., late-December, early-January) there was little or no precipitation. Comparison with Figure 5.7 also shows the lowering of the LCL during large precipitation events (i.e., mid-November and mid-January).

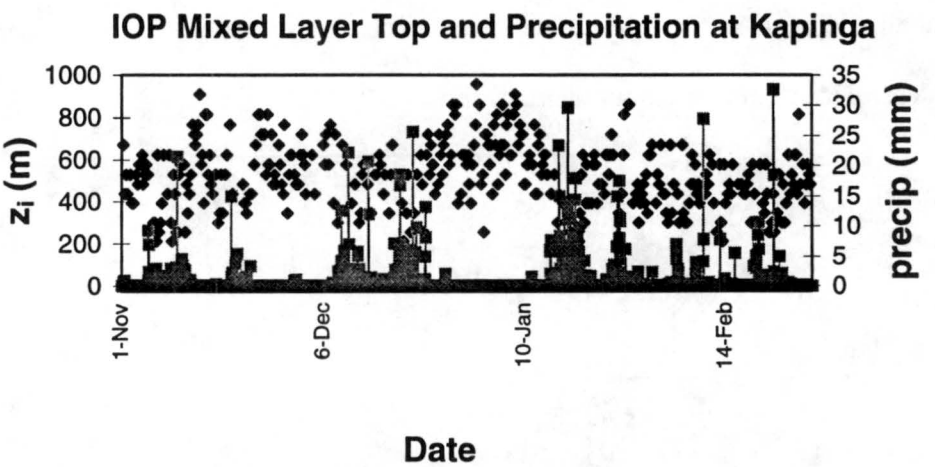

Figure 5.12 Mixed layer tops (diamonds) and precipitation (squares) at Kapinga for the IOP. Precipitation was recorded hourly by an optical rain gauge.

[1] Currently there is some discrepancy regarding the surface moisture values at the Moana Wave. It has been suggested that a 6% correction be applied to the surface data to make it more moist (Chris Fairall, personal communication, 1995).

5.3 Relation Between the Mixed Layer and the Wind Speed

5.3.1 Surface Wind Speed

Figure 5.13 shows the relationship between the mixed layer top and the surface wind speed at Kapinga. Peaks in the wind speed generally occurred when the mixed layer was relatively shallow. Initially, this may contradict the logic that stronger winds promote stronger mixing. However, comparison with Figure 5.12 shows that many, though not all, of the peaks in the surface wind speed corresponded to precipitation events. This supports the idea that convective downdrafts were contributing to the shallow mixed layers and causing an increase in the surface wind.

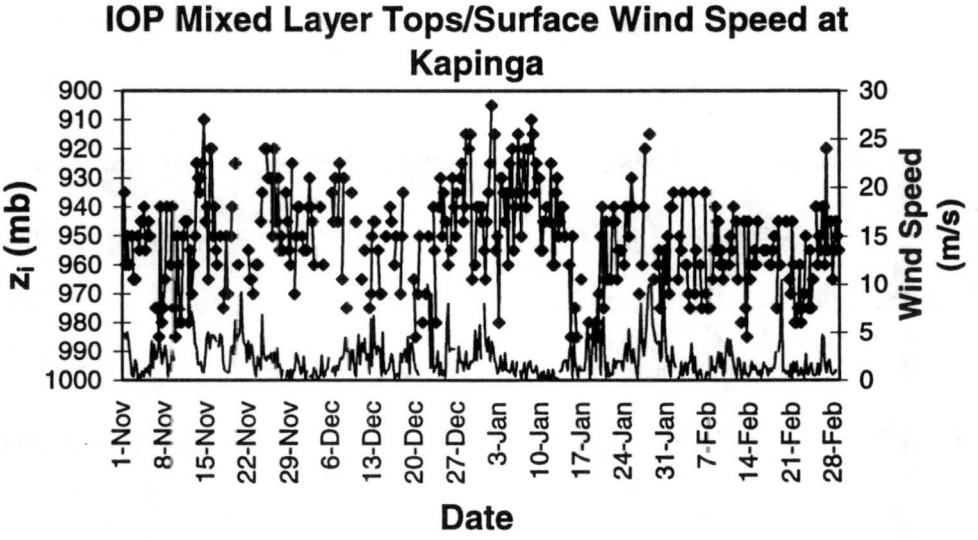

Figure 5.13 Mixed layer tops (diamonds) and surface wind speed (gray solid line) at Kapinga for the IOP.

5.3.2 Westerly Wind Bursts and Longer Time Scales

Three major westerly wind bursts, associated with the 40-50 day oscillation, occurred over the IFA during the four month IOP. The first wind burst took place from the beginning to

the end of November, the second from the middle of December to the beginning of January, and the third from the end of January to the end of February. The entire troposphere, including the boundary layer, was affected by the increase in wind speed. These wind bursts lasted from a few days to a few weeks and interrupted the weak, low-level easterlies that are typically present (Lin and Johnson 1996). The westerly wind burst causes a variation in the SST, sensible and latent heat fluxes, wind speed, and precipitation all of which impact the mixed layer.

It is easy to see why the mixed layer depth is constantly changing. The surface wind fluctuates on short time scales, independent of the westerly wind bursts, as do precipitation events. However, the low-frequency oscillation in the mixed layer depth at Kapinga (Figure 5.1) is a testament of this link to the intraseasonal oscillation. Note that even within these envelopes of long-term variation, the mixed layer varies on short time scales.

The time series presented in this chapter illustrate many features of both the long- and short-term variation. The LCL at Kapinga is the same shape as the z_i time series and generally several hundred meters higher. Convection causes the boundary layer to be disrupted. Therefore, precipitation often corresponds to very shallow mixed layers. Strong surface winds may be indicative of convective downdrafts and again typically accompany shallow mixed layers. Because there were so many convective systems passing through the IFA during TOGA COARE, the simple model illustrating the change in the mixed layer depth with time often does not apply.

Chapter 6

MEAN PROPERTIES OF THE MIXED LAYER

To obtain a more detailed understanding of the mixed layer characteristics, we present histograms of mixed layer tops at each station along with tables outlining various mixed layer and surface statistics. The range of depths for any given station suggest that the mixed layer is not static. Instead, it is constantly adjusting to the changing environment.

6.1 Mean Mixed Layer Properties

Tables 6.1 - 6.4 present statistics for the surface temperature, wind speed, specific humidity, and height of the LCL as well as the mixed layer top for the four sounding stations analyzed. The skewness indicates the degree of asymmetry of the distribution around its mean (Press et al. 1992) and is given by the equation:

$$Skew(x_1 \ldots x_N) = \frac{1}{N}\sum_{j=1}^{N}\left[\frac{x_j - \bar{x}}{\sigma}\right]^3 \tag{6.1}$$

where x is the measured quantity, $\bar{x}$ is the mean, N is the population size, and σ is the distribution's standard deviation. A positive value for skewness indicates a distribution with an asymmetric tail extending towards more positive x while a negative skewness signifies a distribution where the tail extends toward more negative x. According to Press et al. (1992), the standard deviation of equation 6.1 for an idealized normal (Gaussian) distribution is approximately $\sqrt{\frac{15}{N}}$. They advise that skewness is only significant when it is many times as

large as this. Many of the skewness values in Tables 6.1 - 6.4 do not meet this criteria and thus their significance should not be weighted too heavily (for example, for the mixed layer tops at Kapinga, where N is approximately 356, $\sqrt{\frac{15}{N}}$ equals 0.2 which is actually larger than the skewness values in the table). Nevertheless, we have left the skewness values in this study for they give some general insight to the factors that may be affecting the mixed layer depth. Furthermore, we will refer to the apparent skewness that is qualitatively evident in many of the histograms.

6.1.1 Kapinga

As shown in Table 6.1, the mean mixed layer top at Kapinga for the entire IOP was 950.8 ± 16.8 mb. This corresponds to a mixed layer depth of 515.0 ± 155.3 m. The distribution of mixed layer tops is skewed toward lower values due to the frequent occurrence of convection (Figure 6.1). Cold downdrafts associated with convection stabilize the boundary layer and suppress mixing. Mixed layers in the convective wake are very shallow or may even be completely eliminated. The frequent occurrence of mixed layer tops at 940.0 mb (615.7 m) and 945.0 mb (568.9 m) suggests that these values may characterize ambient conditions for regions not effected by convection. Seventy-five percent of the IOP soundings at Kapinga are represented in Figure 6.1 (i.e., 75% showed a detectable mixed layer).

The mean surface temperature at Kapinga was 28.4°C ranging from a minimum value of 23.8°C to a maximum value of 33.0°C with a standard deviation of 1.4°C. The mean surface temperature at Kapinga falls between the mean air temperature and SST at the IMET buoy (27.9°C and 29.4°C respectively, Weller and Anderson 1995) which may indicate that Kapinga was slightly influenced by land.

Kapinga (All Winds)

	Mean	Median	Standard Deviation	Max	Min	Skewness
z_i (mb)	950.8	950.0	16.8	985.0	905.0	-0.1
z_i (m)	515.0	522.0	155.3	203.3	949.5	0.1
T sfc (C)	28.4	28.4	1.4	33.0	23.8	0.2
U (m/s)	2.4	1.8	2.2	13.8	0.0	1.8
q (g/kg)	18.9	19.2	1.3	22.1	14.0	-0.9
LCL (m)	838.3	847.4	180.1	1323.4	289.5	0.3

Table 6.1 IOP statistics for Kapinga. Temperature (T), wind speed (U), and specific humidity (q) are measured at the surface.

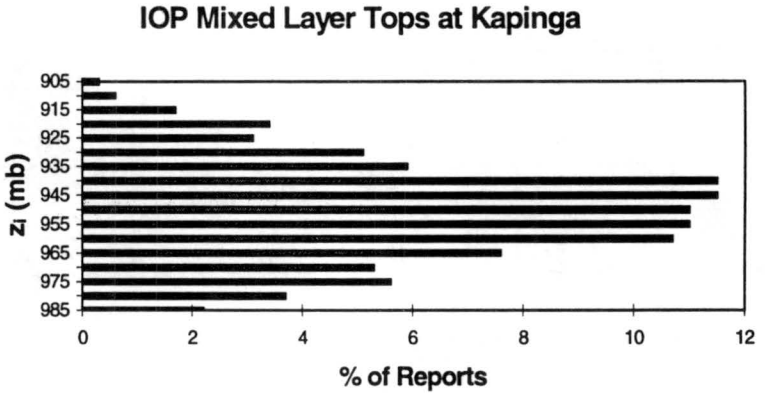

Figure 6.1 Distribution of mixed layer tops at Kapinga for the entire IOP, all times, all cases.

Mean conditions at Kapinga varied with surface wind intensity (Table 6.2). The average wind speed for the entire IOP was 2.4 m/s (Table 6.1), considerably less than that at the IMET buoy (4.3 m/s, Weller and Anderson 1995). It is possible that there was some obstruction to the surface flow at Kapinga due to structures and vegetation on the atoll. There is a strong positive skewness in wind speed, consistent with the idea of frequent high winds and gustiness associated with weak convection. In the absence of convection, as the wind increases, we would expect enhanced mixing and therefore a deeper mixed layer. Table 6.2 shows such behavior for a certain range of wind speeds, but not all. The mean mixed layer top for winds less than 2 m/s was 950.7 mb. For winds between (and including) 2 and 5 m/s, the mean mixed layer top rose to

948.8 mb. Note that the mean surface temperature also increased from 28.4 to 28.7°C. However, for the strongest winds (those greater than 5 m/s) the mean mixed layer was actually shallower -- 958.2 mb -- while the mean surface temperature dropped to 27.7°C, a full degree cooler than the previous category. In this latter category, cool downdrafts, associated with convection, would account for both the increase in surface wind speed and the drop in air temperature as well as the shallower mixed layer depths, i.e., many recovering convective wakes were probably included in the strong-wind category.

Winds < 2 m/s

	Mean	Median	Standard Deviation	Max	Min	Skewness
z_i (mb)	950.7	950.0	15.8	985.0	910.0	0.0
z_i (m)	515.3	522.0	146.5	203.3	901.0	0.1
T sfc (C)	28.4	28.2	1.4	33.0	23.8	0.3
U (m/s)	0.9	0.9	0.5	2.0	0.0	0.3
q (g/kg)	18.6	18.9	1.4	21.0	14.0	-0.8

a.

Winds between (and including) 2 and 5 m/s

	Mean	Median	Standard Deviation	Max	Min	Skewness
z_i (mb)	948.8	950.0	17.8	985.0	905.0	-0.2
z_i (m)	533.1	522.0	166.1	203.3	949.5	0.2
T sfc (C)	28.7	28.6	1.2	31.5	26.0	0.2
U (m/s)	3.1	3.0	0.9	5.0	2.0	0.4
q (g/kg)	19.3	19.4	1.0	21.9	16.6	-0.2

b.

Winds > 5 m/s

	Mean	Median	Standard Deviation	Max	Min	Skewness
z_i (mb)	958.2	960.0	17.9	985.0	915.0	-0.3
z_i (m)	446.5	429.8	164.9	203.3	852.7	0.3
T sfc (C)	27.7	27.9	1.4	29.9	25.1	-0.3
U (m/s)	7.6	6.8	2.0	13.8	5.2	1.1
q (g/kg)	19.6	19.8	0.7	20.7	18.1	-0.5

c.

Table 6.2 Mixed layer statistics at Kapinga for various surface wind speeds: a. for winds less than 2 m/s, b. for winds between (and including) 2 and 5 m/s, and c. for winds greater than 5 m/s. Temperature (T), wind speed (U), and specific humidity (q) are all measured at the surface.

6.1.2 *Moana Wave*, *Ship 3*, and *Ship 5*

The mean mixed layer tops at the *Moana Wave*, *Ship 3* (averaged over all three cruises), and *Ship 5* (cruises 2 and 3) are shown in Tables 6.3 - 6.5 and Figures 6.2 - 6.4. The mean mixed layer tops ranged from 953.9 mb (470.2 m) at *Ship 3* to 948.2 mb (539.5 m) at *Ship 5*. These results indicate that the mean mixed layer depth does not vary significantly throughout the IFA nor, for that matter, throughout the entire tropics (e.g., Fitzjarrald and Garstang 1981; Bond 1992). The histogram of mixed layer tops at *Ship 3* is very similar to that at Kapinga with the tops apparently skewed toward shallower values (to some extent a visual conclusion -- recall that the computed skewness values are not believable compared to the Gaussian standard deviation).

Moana Wave

	Mean	Median	Standard Deviation	Max	Min	Skewness
z_i (mb)	951.4	950.0	16.8	990.0	915.0	-0.1
z_i (m)	510.5	522.0	156.2	852.7	158.7	0.2
T sfc (C)	28.2	28.3	1.0	30.7	24.8	-0.8
U (m/s)	5.4	4.9	2.7	13.8	0.4	0.6
q (g/kg)	17.4	17.5	1.0	20.6	14.6	0.0
LCL (m)	839.3	828.1	155.0	1228.0	438.3	0.1

Table 6.3 Statistics for the *Moana Wave*, all three cruises. Temperature (T), wind speed (U), and specific humidity (q) are measured at the surface.

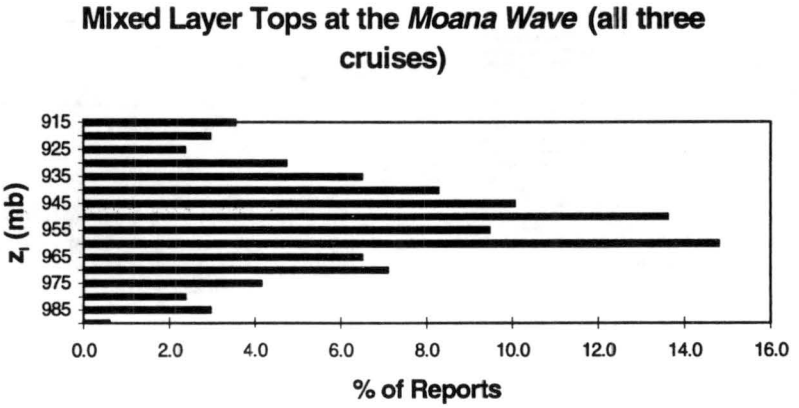

Figure 6.2 Distribution of mixed layer tops at the *Moana Wave*.

Unlike Kapinga and *Ship 3*, *Ship 5* and the *Moana Wave* show a skewness toward deeper mixed layers for reasons we are not yet able to fully understand. There is evidence from the time series of z_i at *Ship 5* and the *Moana Wave* (not shown) that deeper mixed layers occur during non-convective, light-wind episodes and the peak of westerly wind bursts as in the case of Kapinga (Figure 5.9). These periods may be contributing to the skewing of mixed layer depths toward higher values (e.g., note the peak at 930 mb at *Ship 5*).

Ship 3

	Mean	Median	Standard Deviation	Max	Min	Skewness
z_i (mb)	953.9	950.0	17.6	995.0	900.0	0.2
z_i (m)	470.2	504.5	162.6	980.8	96.9	-0.2
T sfc (C)	28.3	28.5	1.0	30.8	24.3	-1.2
U (m/s)	4.8	4.2	4.1	38.5	0.1	4.7
q (g/kg)	18.1	18.3	1.1	20.2	14.2	-1.0
LCL (m)	736.3	743.5	152.0	1178.0	265.6	0.0

Table 6.3 Statistics for *Ship 3*, all three cruises. Temperature (T), wind speed (U), and specific humidity (q) are measured at the surface.

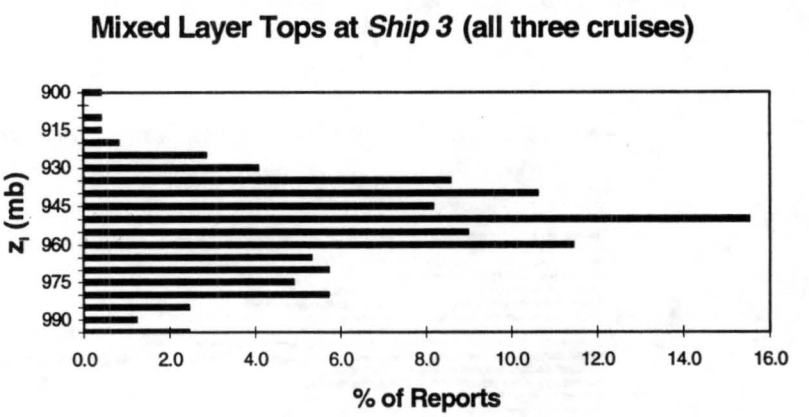

Figure 6.3 Distribution of mixed layer tops at *Ship 3*.

Ship 5

	Mean	Median	Standard Deviation	Max	Min	Skewness
z_i (mb)	948.2	950.0	15.5	985.0	910.0	-0.0
z_i (m)	539.5	522.0	144.5	901.0	203.3	0.1
T sfc (C)	28.4	28.4	0.8	33.0	25.4	0.8
U (m/s)	5.3	4.9	2.7	16.0	0.4	1.0
q (g/kg)	18.5	18.8	1.3	20.4	12.3	-2.1
LCL (m)	858.0	851.3	150.3	1501.2	407.7	0.5

Table 6.4 Statistics for *Ship 5*, cruises 2 and 3. Temperature (T), wind speed (U), and specific humidity (q) are measured at the surface.

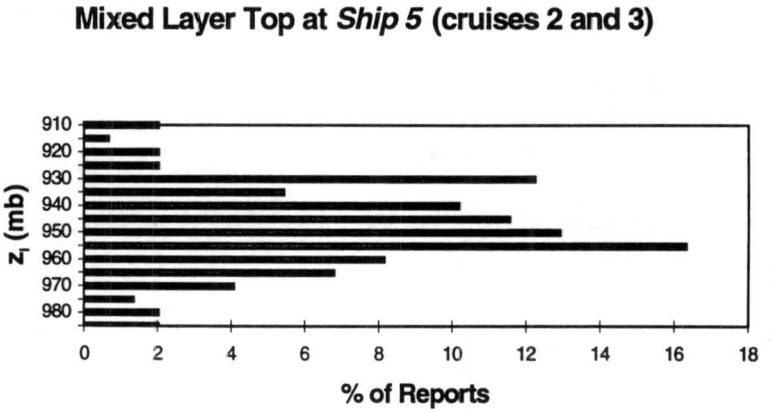

Figure 6.4 Distribution of mixed layer tops at *Ship 5*.

If the only process disrupting the ambient mixed layer depth was the occurrence of convective wakes, we would expect to see the mixed layer tops, surface temperature, and surface specific humidity skewed toward smaller values and the wind speed skewed toward larger values. As in the case of Kapinga, the skewness values for wind speed (U) are positive at all three other sites while specific humidity (q) is consistently negative. Although skewness values for the temperature and the mixed layer top may vary from site to site, the wind and moisture data generally indicate the occurrence of convective wakes.

Notice the mean winds at the ship sounding sites were considerably higher than that at Kapinga ranging from 4.8 m/s at *Ship 3* to 5.4 m/s at the *Moana Wave*. These values are much

closer to that found at the IMET buoy and support the hypothesis that there was some obstruction to the surface wind flow at Kapinga, although it is also possible that the mean wind speed was actually weaker there owing to a peaking of westerly wind bursts to the south of the equator (e.g., Lin and Johnson 1996).

6.1.3 Histograms

Another informative way to illustrate the surface properties outlined in the above tables is through histograms. Figures 6.5 and 6.6 show the distribution of the surface temperature and wind speed at Kapinga for all times. The surface temperatures are fairly evenly distributed about the mean with the coolest values most probably occurring in the wake of convection. Again note the small wind speeds at Kapinga and the prominent skewness toward higher wind speeds.

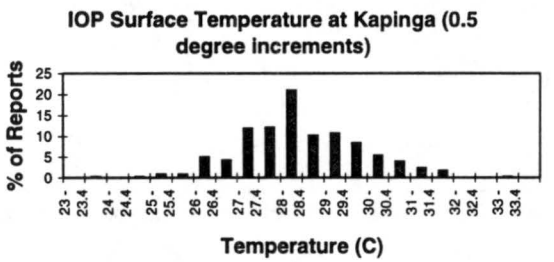

Figure 6.5 Histogram of the surface temperature at Kapinga for the IOP.

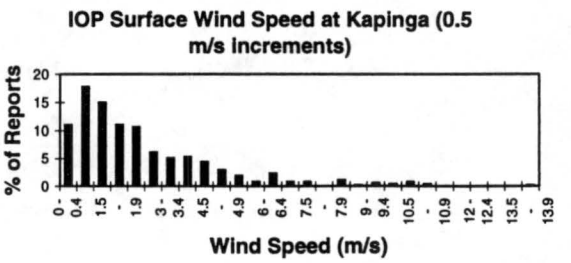

Figure 6.6 Histogram of the surface wind speed at Kapinga for the IOP.

The scatter plot of mixed layer top versus mixed layer mean θ (Figure 6.7) generally shows a positive correlation between the two (although the correlation is weak for $\theta > 301^{\circ}K$). Note that when the boundary layer was the coolest ($\theta < 300^{\circ}K$) the mixed layer was shallow (tops below 960 mb). Precipitation was occurring when many of these shallow mixed layers

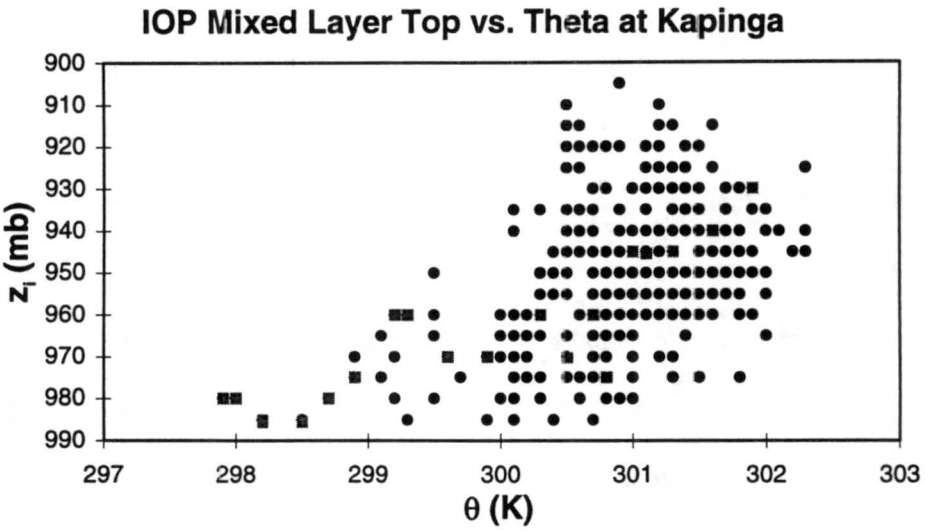

Figure 6.7 Mixed layer tops at Kapinga versus the mean potential temperature in the mixed layer. The light boxes indicate times when precipitation was occurring within an hour of the observation.

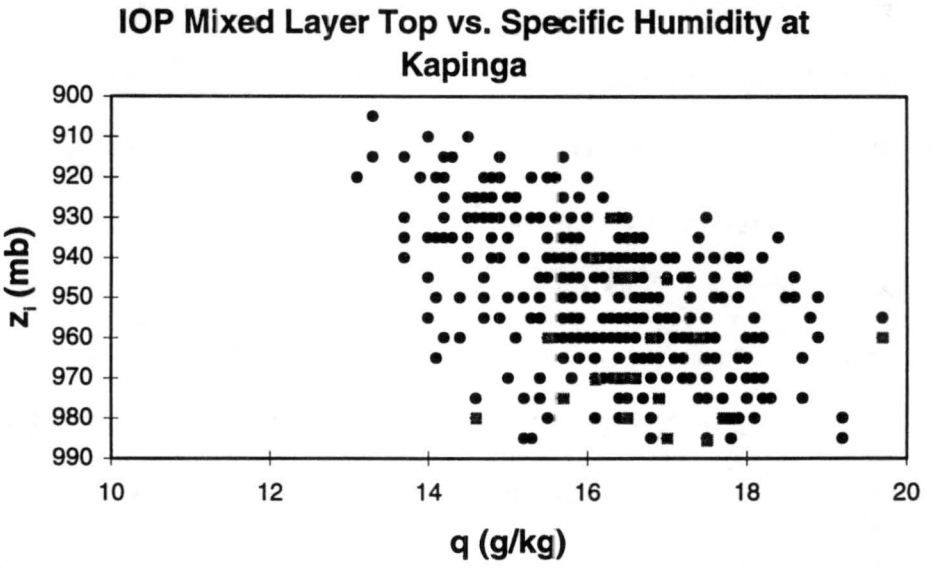

Figure 6.8 Mixed layer tops at Kapinga versus the mean specific humidity (q) in the mixed layer. The light boxes indicate times when precipitation was occurring within an hour of the observation.

existed as indicated by the lighter circles. This again supports the importance of convective downdrafts on the atmospheric boundary layer at Kapinga.

A similar plot shows the mixed layer top versus the mean specific humidity in the mixed layer (Figure 6.8). In this case, the two variables are negatively correlated with the shallow mixed layers somewhat moister (higher q) than the deep ones. This finding is consistent with the idea that deeper mixed layers entrain progressively drier air from aloft. There was a slight preference for precipitation to be associated with the shallower mixed layers; however, the magnitude of q did not seem to correlate with the rainfall. This may indicate the occurrence of both moist and dry downdrafts in convective systems.

It has been suggested by Dave Parsons (personal communication, 1996) that mixed layer growth may be correlated to dry intrusions. Whether or not this speculation is true, it is logical to expect that mixed layers during dry intrusions should be drier than the mean. Both these ideas appear to be borne out by the observations. Dry intrusions occurred frequently during the IOP (Figure 6.9 from Mapes and Zuidema 1996). Comparing the occurrences of dry intrusions at low-levels from Mapes and Zuidema to the mixed layer depth, there was a tendency for the mixed layer to be deeper and drier during these dry episodes (Figures 6.9 and 6.10).

Also, Figure 6.10 shows numerous times when the specific humidity dropped and the mixed layer deepened. Note that these times correspond to low-level dry intrusions shown in Figure 6.9 (e.g., the humidity drops near days 12, 68, and 85).

Fitzjarrald and Garstang (1981) also found that drying in the atmosphere above the mixed layer tends to be accompanied by thicker mixed layers. The relationship between the two, however, is still unclear. The dry intrusions may simply be a mechanism that inhibits convection, thereby allowing the mixed layer to grow due to the absence of precipitation and convective wakes (i.e., clear-sky conditions). Dry intrusions as a primary growth factor are not conclusive but remains an important area of research.

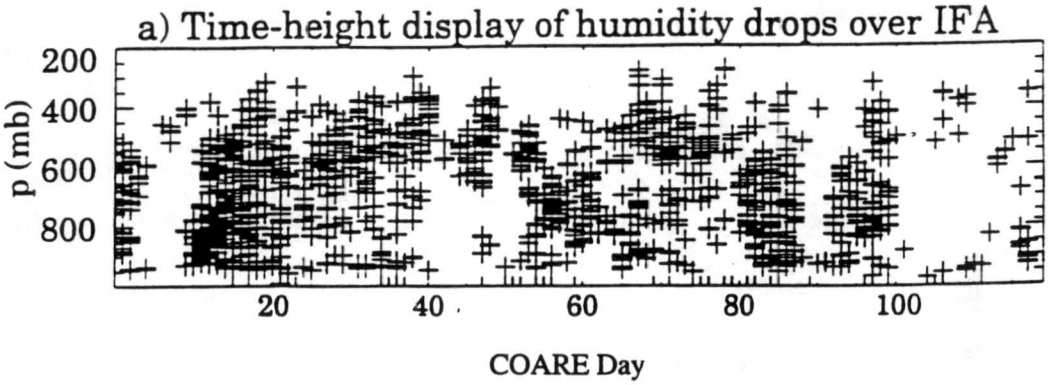

Figure 6.9 Time-height display of humidity drops at the stations making up the COARE Intensive Flux Array (IFA). Figure is from Mapes and Zuidema (1996).

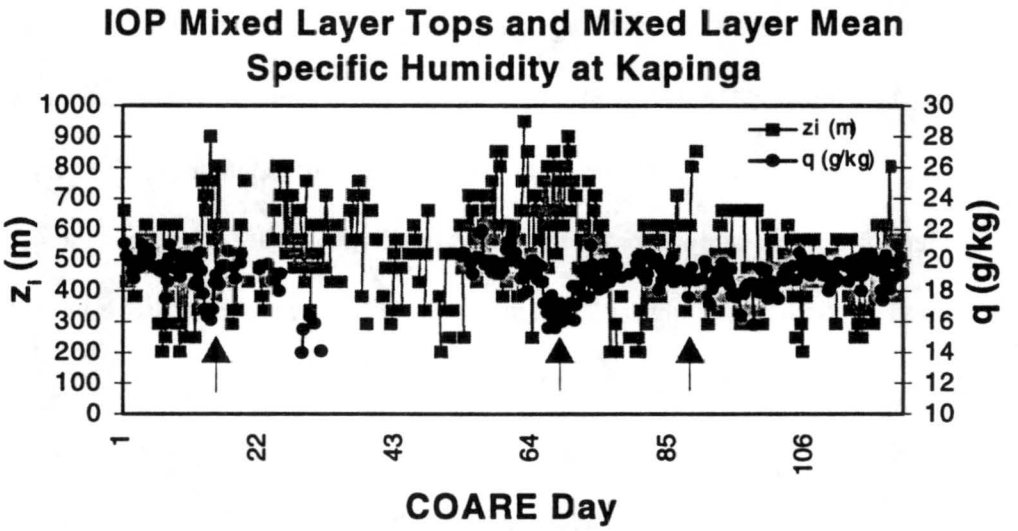

Figure 6.10 Time series of mixed layer tops (squares) and specific humidity (circles) at Kapinga for the IOP. Arrows indicate examples of when drops in specific humidity accompanied deep mixed layers.

6.2 Mixed Layer Structure

To further analyze the structure of the mixed layer, we created mean normalized soundings for Kapinga, *Ship 3*, *Ship 5*, and the *Moana Wave*. To create each mean sounding, we first scaled the data by z_i. This procedure normalizes the soundings in order to preserve the mixed layer structure. Next, we divided the mixed layer into tenths of z_i (with the mixed layer top equal to $1.0z_i$). The corresponding levels from all the soundings were then averaged to create a mean profile up to $1.4z_i$. This range illustrates both the mixed layer and the capping entrainment zone. Note that this procedure was not designed to preserve the structure of the entrainment zone. However, the entrainment zone is detectable in nearly all of the mean soundings with a top (z_t) approximately between 1.1 and 1.2 z_i. Although exact scaling of the entrainment zone would have been informative, it was often impossible to determine z_t from the 5 mb interpolated sounding data. Johnson (1977) employed a similar scaling process in a study of the mixed layer over south Florida.

The mean sounding at Kapinga shows a very well-mixed layer in both θ and q up to the mixed layer top at 515 m (1.0 z_i) (Figure 6.11). The θ sounding suggests a weak superadiabatic layer near the surface -- a feature seen in many individual soundings. The very moist surface values of q are possibly a consequence of errors in the surface moisture data.

Initially, soundings at Kapinga (and Nauru) experienced low-level moisture errors due to launching the balloons from air-conditioned vans. This produced unrealistically small values of q. When these errors are corrected, a peak in surface moisture appears instead. According to Cole (1993), the very rapid decrease in q from the surface to the first ten-second sonde measurement is likely due to an inaccurate calculation of the humidity sensor time constant. According to the report, the Vaisala radiosonde specifications give a humidity time constant of 1 second for a flow rate of 6 m/s and a pressure of 1000 mb. It is believed that the humidity errors were a result of the time constant being calculated before adding the protective cap (Cole 1993).

Furthermore, sondes at Kapinga were typically laid on the ground to record surface values before being brought into the van for launching. The heating of the sondes when placed in the sun would also cause higher moisture readings, especially when compared to the moisture values it recorded in the cool, dry van. These errors seem to be confined to the lowest 50-100 m. In the figures, data that are not considered reliable are denoted by a dashed line. Values above this level do not appear to be significantly affected.

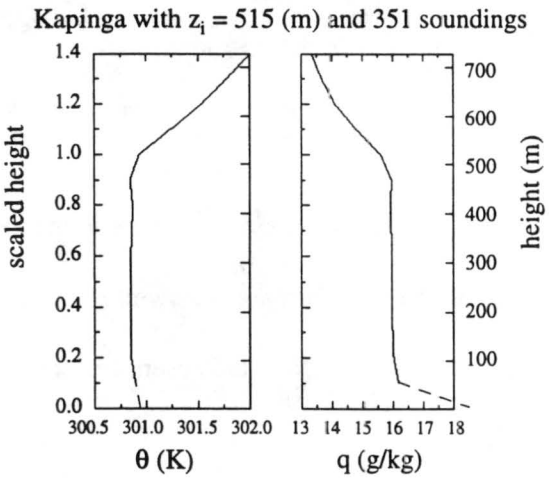

Figure 6.11 Mean sounding for Kapinga

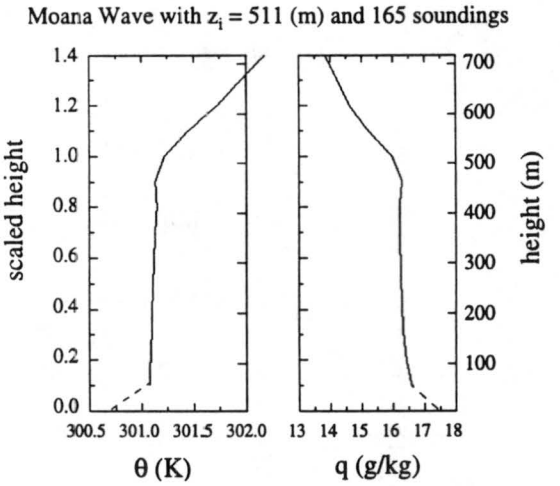

Figure 6.12 Mean sounding for the *Moana Wave*

Note that θ actually begins to increase roughly 50 m beneath z_i while q begins to falloff at the same point (a feature also found by Mahrt 1976; Fitzjarrald and Garstang 1981). Above z_i, an entrainment zone of approximately 100 m depth is perceptible. This depth is in agreement with the mean entrainment zone thickness found by Fitzjarrald and Garstang (1981) and LeMone and Pennell (1974). It is interesting to note that while the scaling procedure was not designed to preserve the entrainment zone structure, some evidence for it still exists at approximately 1.1-1.2 z_i. The fact that it is still detectable indicates that the entrainment zone is a persistent feature.

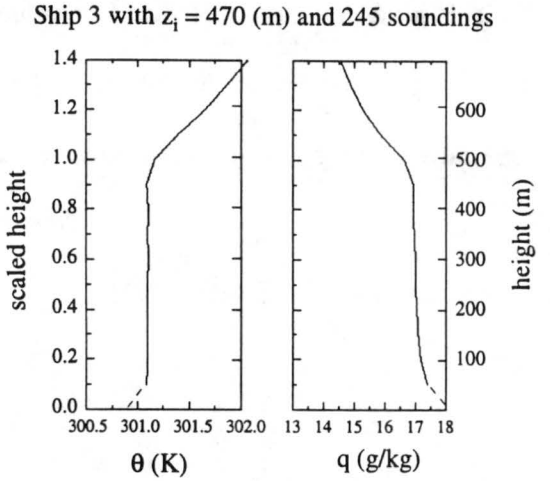

Figure 6.13 Mean sounding for *Ship 3*

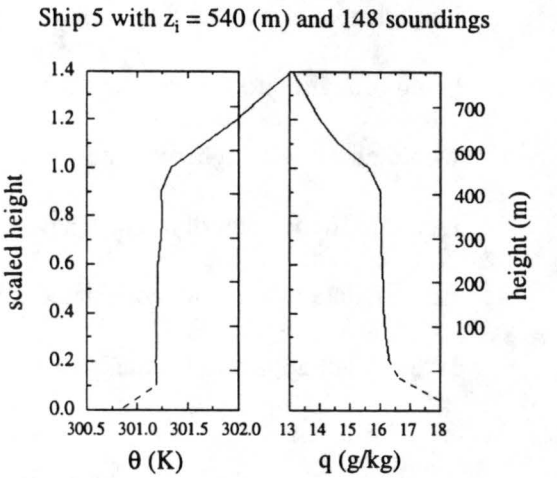

Figure 6.14 Mean sounding for *Ship 5*

The mean sounding from the *Moana Wave* (Figure 6.12) is very similar to the mean sounding calculated at Kapinga. Again, both the θ and q profiles are very well-mixed up to z_i. In this case, the mean z_i is 511 m -- only 4 m less than Kapinga. Note the absence of the large moisture spike at the surface of the q sounding.

Soundings from *Ship 3* (Figure 6.13) and *Ship 5* (Figure 6.14) also produce similar mean soundings. The mean z_i at *Ship 3*, 470 m, is somewhat shallower than at Kapinga and the *Moana Wave*. In contrast, *Ship 5* has the deepest mean mixed layer depth at 540 m. Fitzjarrald and Garstang (1981) found the mean mixed layer top to be 424 m in GATE. This slightly smaller mean is possibly explained by the cooler SSTs in the Atlantic (however, other factors, such as wind, frequency of rainfall, and others may also come into play).

Comparing all three mean soundings, Kapinga is both the coolest and the driest with a mean θ of 301.1°K and a mean q of 15.4 g/kg (excluding the surface q value). *Ship 5* is the warmest and the moistest with a mean theta of 301.3°K and a mean q of 16.5 g/kg (also excluding the surface value). Results from this study are in general agreement with the findings

of Walt Petersen (personal communication, 1996) who looked at the specific humidity at various ship stations. He found the mean q at the *Moana Wave* to be 16.0 g/kg.

6.3 Mean Soundings for Various Depth Ranges

The relationship between z_i and the mean θ and q in the mixed layer becomes more apparent when mean soundings for various categories of mixed layer depths are created. At each station, we divided the data into four groups. At Kapinga, mean soundings were created for mixed layers with tops ranging from 985-970 mb (60 soundings), 965-950 mb (141 soundings), 945-930 mb (117 soundings), and 925-905 mb (32 soundings). This is essentially isolating the shallowest and the deepest quartiles of mixed layer tops and dividing the middle group into two (see figure 6.15).

The mean z_i for the shallowest mixed layers was 288 m. As expected, considering the effects of downdrafts, these mixed layers were substantially colder than the mean sounding for all cases. The shallow mixed layers were also relatively moist. For z_i values from 965-950 mb, the mean z_i increased to 462 m and the mean potential temperature increased by nearly a degree. The next deepest category (945-930 mb) again shows an increase in the mean potential temperature in the mixed layer. The mean z_i for this group was 624 m. For the deepest mixed layers, 925-905 mb, the mean z_i was 803 m. Here the mean potential temperature in the mixed layer actually decreased from the value in the previous category. However, the specific humidity markedly decreased for these deep layers. This suggests that the deeper mixed layers are entraining drier air from above. The decrease in q and increase in θ in the upper one-third of the mixed layer for the deepest category supports the concept of dry air entrainment in those cases (e.g., Mahrt 1976).

Figure 6.16 shows the same plot but for the *Moana Wave*. Here the divisions were from 990-975 mb (17 soundings), 970-955 mb (65 soundings), 950-935 mb (65 soundings), and 930-

915 mb (23 soundings). The same behavior seen in the Kapinga figure also applies to the *Moana Wave* with the shallowest mixed layers being the coldest and the moistest and the deepest the warmest and the driest.

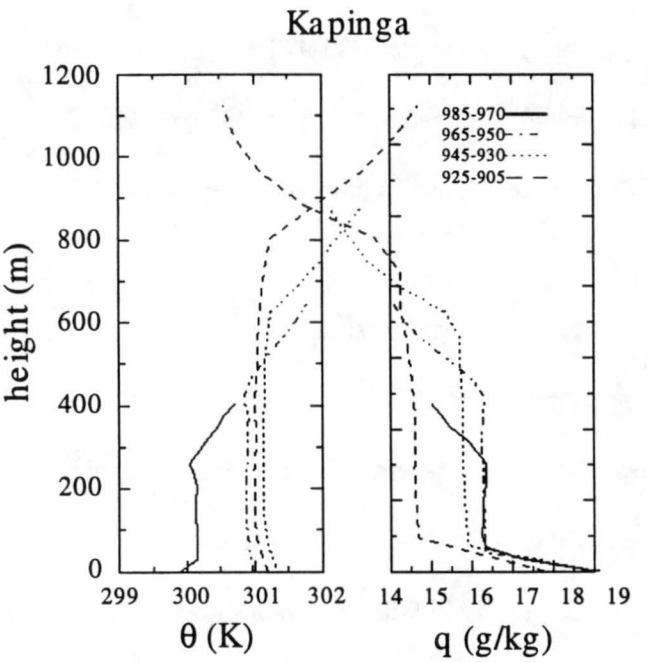

Figure 6.15 Mean soundings at Kapinga for various depth ranges.

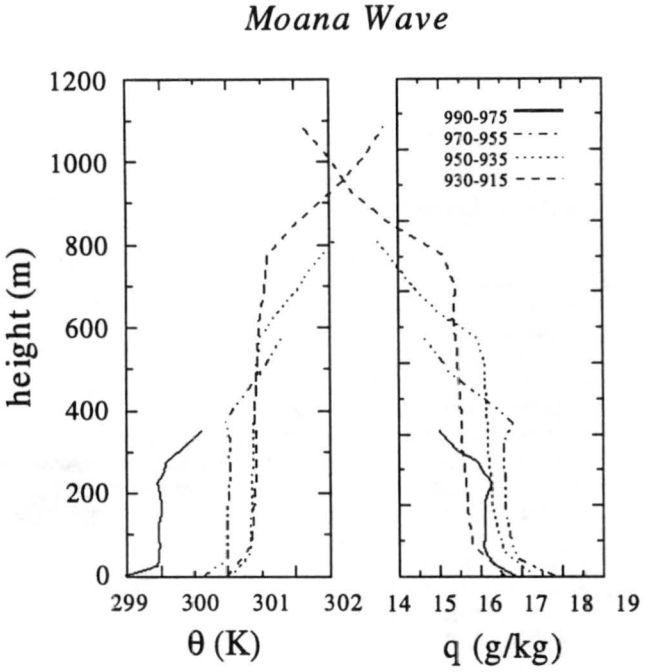

Figure 6.16 Similar to Figure 6.15 but for the *Moana Wave*.

6.4 Light- Versus Strong-Wind Conditions

The wind speed in the boundary layer can profoundly effect the mixed layer. Light-wind, clear sky conditions allow the mixed layer to grow due to enhanced radiational heating. Although strong winds may promote mixing and thus create deeper mixed layers, strong downdrafts can act in the opposite direction by destroying the mixed layer, which eventually recovers over a period of hours or longer.

Figure 6.17 shows the distribution of mixed layer tops at Kapinga, this time for winds less than 2 m/s. Since the IOP mean surface wind speed at Kapinga was 2.4 m/s, this subgroup represents a large portion of the total and therefore greatly resembles the IOP mean statistics (Table 6.1). However, this distribution is not as heavily weighted toward the shallow mixed layers. Theoretically, light-wind periods should have more normal (Gaussian) distributions as

they contain fewer incidences of convective downdraft effects. There are several occasions, however, when light winds can occur in convective wakes (e.g., Johnson and Nicholls 1983).

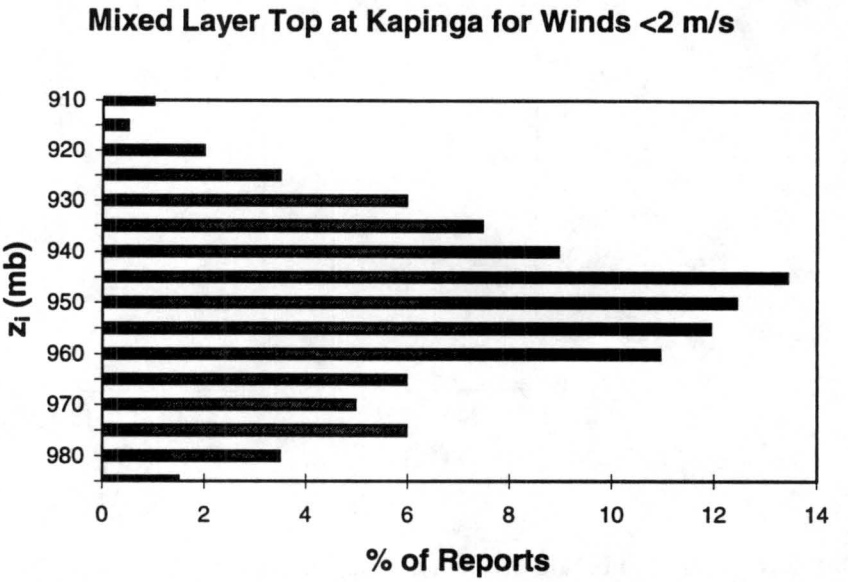

Figure 6.17 Mixed layer tops at Kapinga for winds less than 2 m/s.

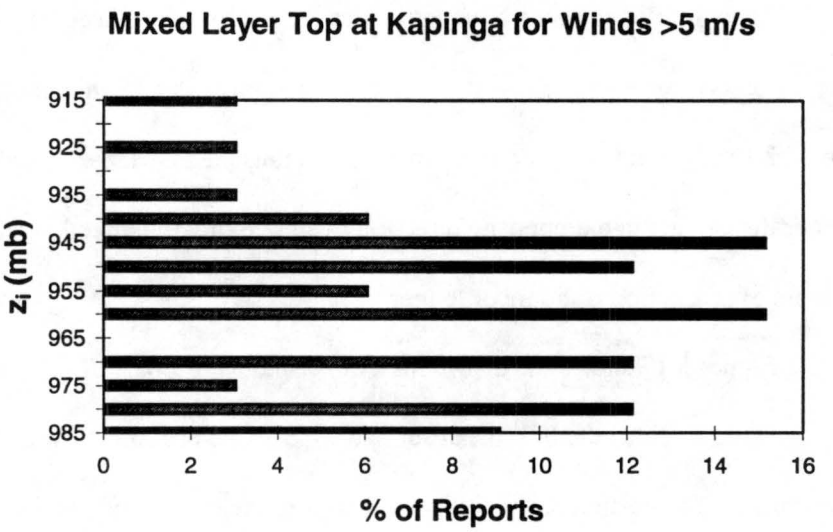

Figure 6.18 Mixed layer tops at Kapinga for surface wind speeds greater than 5 m/s. (See also Table 6.2.)

For comparison, Figure 6.18 shows the histogram of mixed layer tops at Kapinga for winds greater than 5 m/s. The sample size for this plot is much less than that for winds less than 2 m/s. Nevertheless, the mean mixed layer top is notably lower at 958.2 mb (446.5 m) and the distribution indicates a definite skewness towards the shallow mixed layers (presumably recovering boundary layer wakes).

To analyze the mean structure in a relatively undisturbed atmosphere, a mean sounding was created at Kapinga from November 27 - December 7 (Figure 6.19). During this period, the winds were relatively light with an average surface wind speed of 1.1 m/s. Also note the relatively warm brightness temperatures during this time (Figure 6.20). The warm brightness temperatures, lack of precipitation (Figure 5.8), and light surface winds make this case a good example of undisturbed conditions at Kapinga.

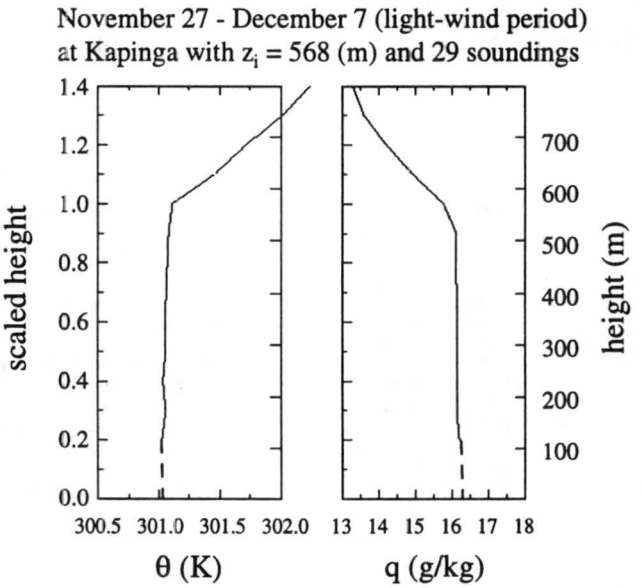

Figure 6.19 Mean sounding at Kapinga for a light-wind period. Dashed line indicates the best estimate of potentially unreliable data in the lowest 100 m.

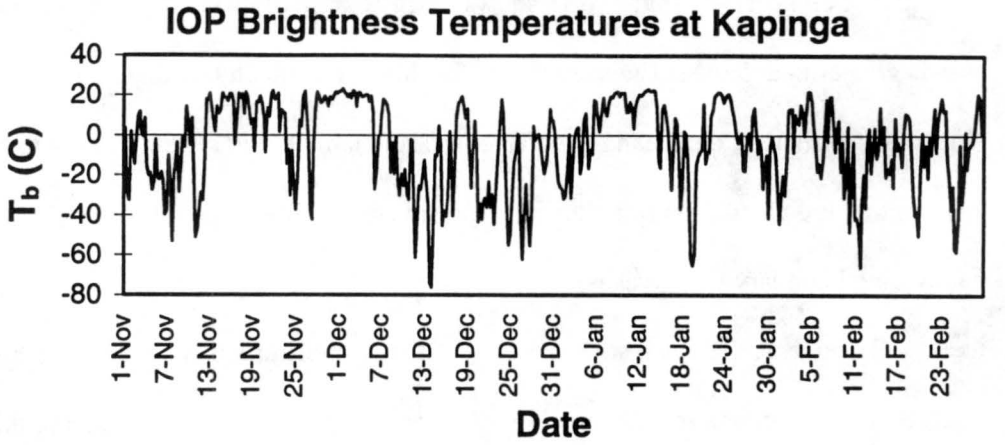

Figure 6.20 IOP brightness temperatures at Kapinga.

The resulting mean sounding shows a mean z_i of 568 m (compared to the mean z_i for all times of 515 m). The increase in z_i suggests that the equilibrium mixed layer depth is considerably greater in the absence of convection. In addition to the enhanced radiational heating in clear-sky conditions, the boundary layer is free from the cold downdrafts associated with mesoscale convective systems that suppress or eliminate the mixed layer.

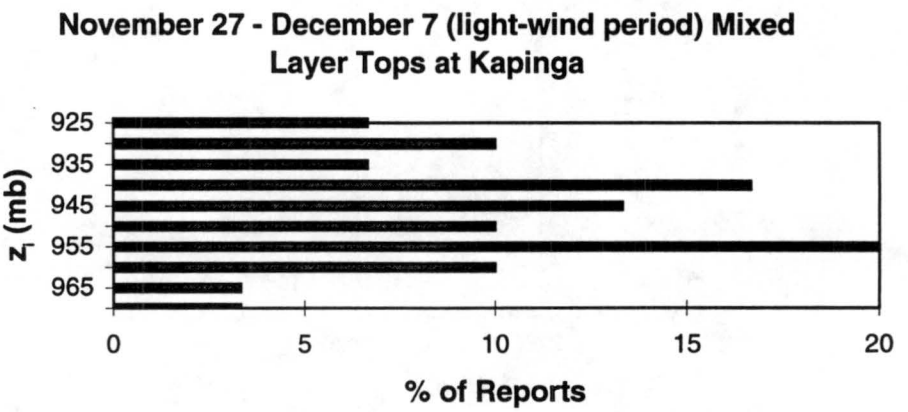

Figure 6.21 Histogram of mixed layer depths at Kapinga for the light-wind period November 27-December 7.

Figure 6.21 is the distribution of the mixed layer tops during the November 27 - December 7 period. Note the absence of mixed layers below 970 mb. The scarcity of shallow mixed layers corresponds with the lack of precipitation events, and thus convective downdrafts, during this period.

At *Ship 3*, we created mean soundings for a light- and strong-wind period (Figures 6.22 and 6.23). Again the mean mixed layer top increased for the light-wind case with z_i equal to 499 m (recall the overall mean at *Ship 3* was 470 m). Although Figure 6.18 showed a predominance of shallow mixed layers at Kapinga for strong wind cases, the mean mixed layer was much higher at *Ship 3* during the strong wind period. During the strong wind period in question at *Ship 3* (December 25 - January 1) there was very little precipitation. Thus, the mixed was not contaminated by convective downdrafts. In the absence of disrupting precipitation, the strong winds enhanced mixing and allowed the boundary layer to grow.

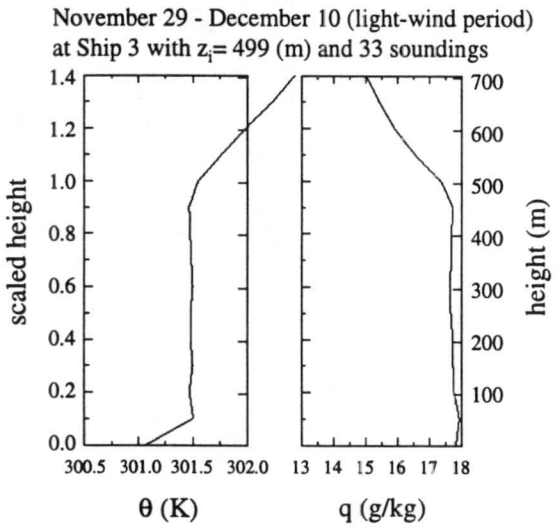

Figure 6.22 Mean sounding for the light-wind period November 29 - December 10 at *Ship 3*.

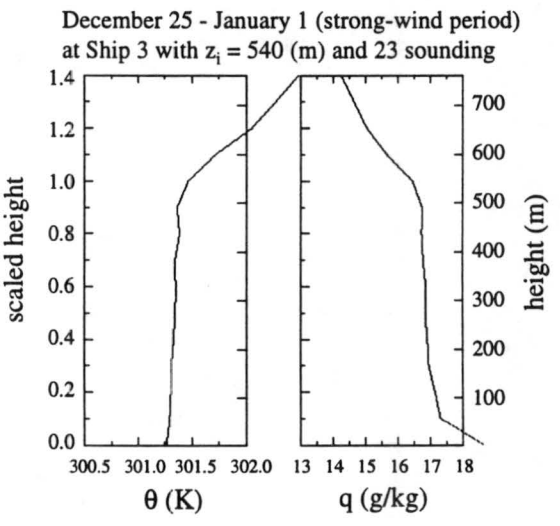

Figure 6.23 Mean sounding for the strong-wind period December 25 - January 1 at *Ship 3*.

The mean profiles and statistics presented here indicate that the IOP mean z_i is approximately the same at all four stations. The structure itself is similar with θ and q well-mixed vertically up to z_i, although θ increases and q decreases in the upper third of the mixed layer for the deepest mixed layers, suggesting significant dry-air entrainment in those cases. Distributions of the mixed layer tops at two sites (Kapinga and *Ship 3*) tend to show a skewness towards shallower mixed layers. This is most likely due to the presence of convective wakes that cool the boundary layer and lead to shallower, recovering mixed layers. Two other sites (*Moana Wave* and *Ship 5*) indicate weak skewness toward deeper mixed layers, which are likely associated with non-convective light-wind conditions and westerly wind bursts. When precipitation is occurring, the mixed layer is typically lower. Shallow mixed layers tend to be cooler and more moist than deeper layers. For isolated light-wind periods, the mean mixed layer is deeper; however, the same well-mixed structure persists.

Chapter 7

DIURNAL CYCLES

Diurnal variability of the boundary layer is common over land due to the inability of the land to store energy. Such a trend is not obviously apparent over the ocean where the sea surface temperature is normally thought to remain fairly constant throughout the day. However, Weller and Anderson (1995) observed a diurnal variation in SST (up to 3°C on clear, light-wind days) and surface fluxes at the IMET buoy during COARE, especially during light-wind conditions. Therefore, one might expect a related, weak but not negligible, diurnal variation in the atmospheric mixed layer depth with maximum depths in the afternoon and minimum at night. Observations from the IFA support this hypothesis.

By averaging all the data for each 6 hour interval (i.e., 00 UTC, 06 UTC, 12 UTC, and 18 UTC), we constructed diurnal plots of various quantities for a given station and time period. Graphs of the diurnal variation in mixed layer potential temperature and specific humidity were computed by averaging the mean θ and q of the mixed layer at each time. Thus, the graphs represent the diurnal variation of the mean θ and q in the mixed layer.

7.1 Variation in the Mixed Layer Top

Figure 7.1 shows the diurnal variation in z_i at Kapinga by plotting the IOP mean mixed layer top every 6 hours. In addition to the means, the standard deviation and the extremes are also plotted at each time.

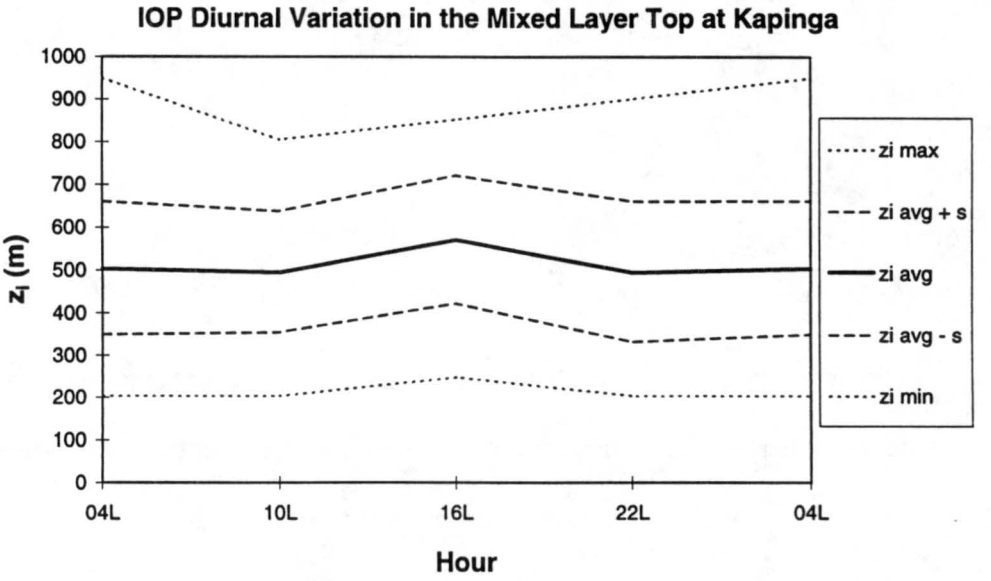

Figure 7.1 Diurnal variation of the mixed layer top at Kapinga. The solid black line is the mean mixed layer top at each time for the IOP. The long-dashed lines denote the standard deviation and the short-dashed lines the extremes at each time.

As expected from the study of Weller and Anderson (1995) showing an afternoon maximum in SST and surface sensible and latent heat fluxes, the deepest mixed layer occurs in the afternoon (16L) (top ~945 mb or 578 m) and the shallowest occurs at 22L (953 mb or 503 m). These amount to approximately a 15% variation in depth throughout the day.

The diurnal variation observed at Kapinga is not exclusive to that location. Figure 7.2 shows the diurnal cycle in mixed layer depth at the *Moana Wave*, *Ship 3*, and *Ship 5*, (data are for all three cruises at the *Moana Wave* and *Ship 3*, cruises 2 and 3 at *Ship 5*). Notice in all four plots the deepest mixed layer occurs in the afternoon when surface fluxes are the greatest (Figure 10, Weller and Anderson 1995). The time of minimum mixed layer depth varies from station to station occurring at either 04L or 22L. Note that since these plots are for all times, there is contamination from storms, showers, etc. In general, the shape of the Kapinga and *Moana Wave* histograms are very similar. *Ship 3* illustrates the most ideal diurnal cycle.

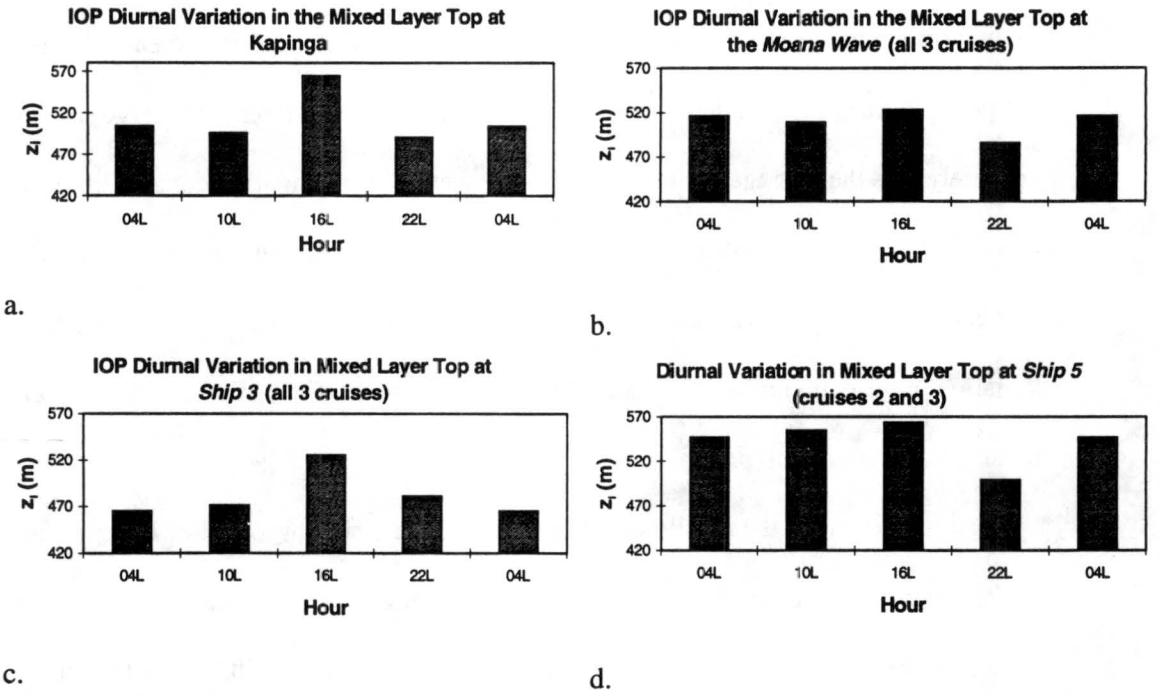

Figure 7.2 Diurnal variation in the mixed layer tops at: a. Kapinga, b. *Moana Wave*, c. *Ship 3*, and d. *Ship 5*.

7.2 Precipitation

To aid in interpretation of the diurnal cycle of the mixed layer, an analysis has been undertaken of the diurnal variation in precipitation during TOGA COARE. While four months of data are not sufficient to determine the diurnal cycle with a high degree of accuracy, some indications of its behavior can be obtained. Gray and Jacobson (1977) studied the diurnal variation of deep convection in the western Pacific using climate data from 1961 - 1973. They found a significant early morning maximum in precipitation between 03L and 06L with an evening minimum between 18L and 23L. Looking only at large islands, Gray and Jacobson found an afternoon maximum in rainfall that is not present on the smaller atolls. They attributed this behavior to a heat island effect.

Maxima in precipitation at Kapinga for the entire IOP did, in fact, tend to occur in the early morning hours and the late afternoon (Figure 7.3). Figure 7.3 was created by averaging all the precipitation amounts that occurred at each hour. Therefore, one very large rain event could adversely bias the average value for that hour, given the four-month record. Furthermore, the precipitation data were not separated into intense versus weak oceanic convection. Gray and Jacobson (1977) found a strong diurnal cycle in intense convection but little or no diurnal variation in weak precipitation. Therefore, in their analysis, Gray and Jacobson (1977) did not include light, stratiform precipitation.

Nevertheless, the results shown in Figure 7.3 are similar to that of Petersen and Rutledge (1996) who looked at the diurnal cycle of rainfall over a sector of the ocean larger than, but encompassing, the IFA (Figure 13, Petersen and Rutledge 1996). They found the maximum rainfall occurred between 02L and 04L with a daily minimum between approximately 09L and 13L. A broad, secondary maximum in rainfall occurred throughout the afternoon.

This diurnal variation in precipitation may influence the diurnal cycle of mixed layer depths shown earlier. For example, since those results are for all times of the IOP, part of the diurnal cycle in z_i may be due to more rain at night (producing shallower mixed layers). In order to remove precipitation effects, an analysis of the diurnal cycle of the mixed layer depth during an undisturbed, light-wind period has been conducted and will be reported later in this chapter.

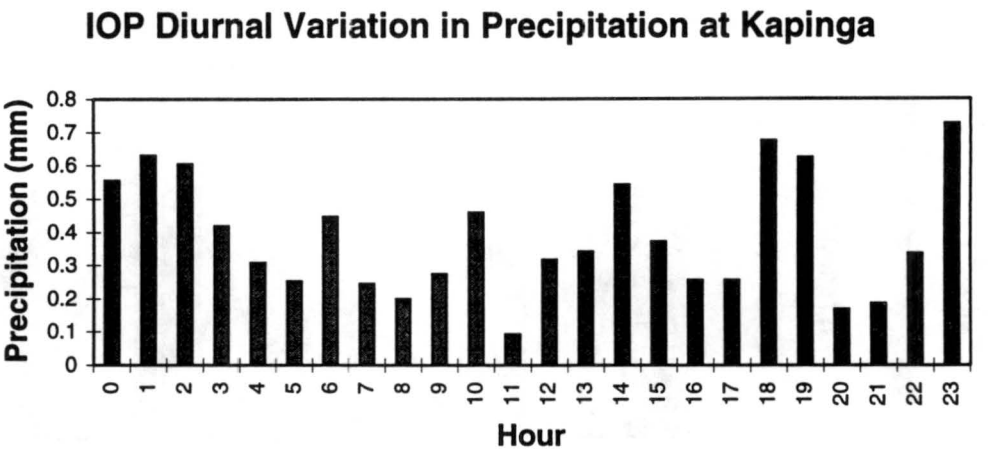

Figure 7.3 Diurnal variation in the hourly precipitation at Kapinga for the IOP. The figure represents the average precipitation amount for all cases at each time.

7.3 Thermodynamic Variation

The diurnal variation in specific humidity (Figure 7.4) shows a minimum in q when the mixed layer is the deepest (16L). This conforms with the concept of deeper afternoon mixed layers entraining drier air from above. Note the total variation in q is within 0.5 g/kg.

For comparison, Figure 7.5 is the q variation at the *Moana Wave* for all three cruises. Unlike Kapinga, this figure does not show any evidence of the dry afternoon mixed layers. However, the *Moana Wave* had considerably fewer soundings than Kapinga. Therefore, the means may have been substantially influenced by precipitation events. Isolating undisturbed periods may show evidence of dry, deep mixed layers, but the limited record of the *Moana Wave* make it difficult to obtain a statistically significant sample size of undisturbed cases.

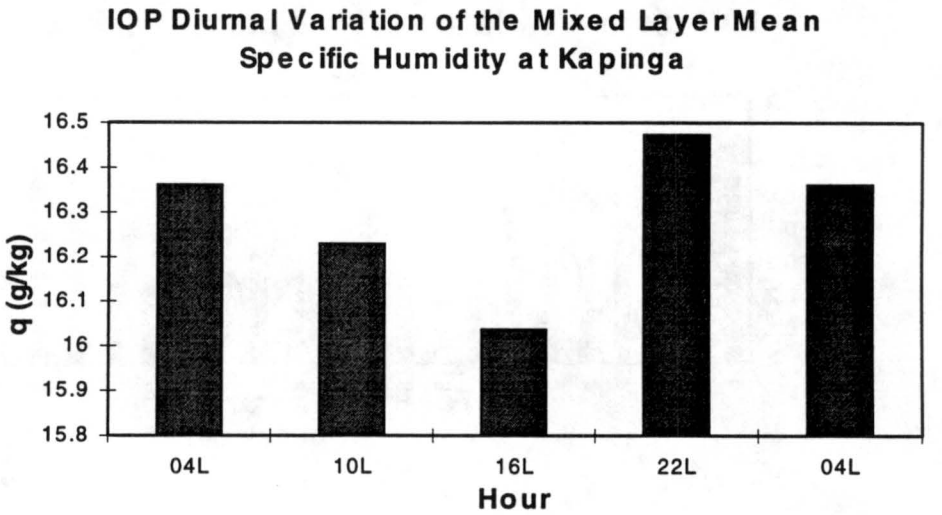

Figure 7.4 Diurnal variation in the mixed layer mean specific humidity at Kapinga for the IOP.

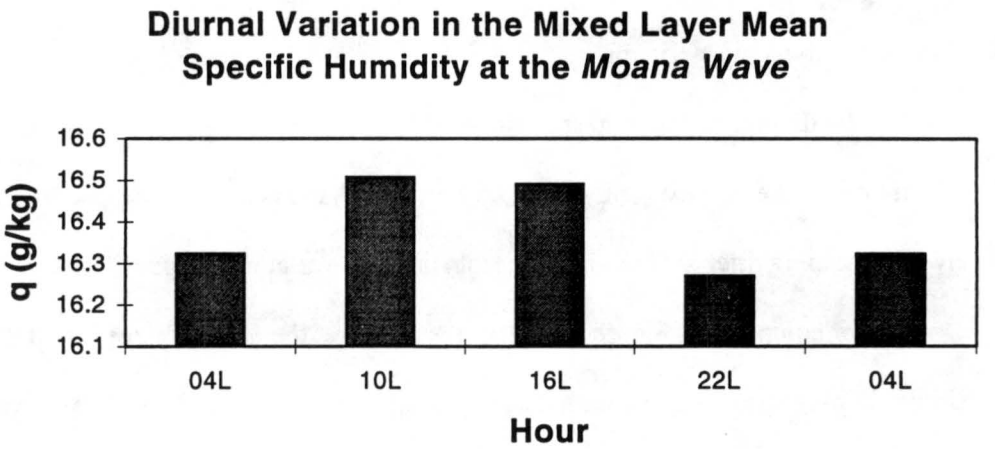

Figure 7.5 Diurnal variation in the mean specific humidity at the *Moana Wave* for all three cruises.

Figure 7.6 shows the diurnal variation in the mean potential temperature ($\overline{\theta}_v$) in the mixed layer at Kapinga for the entire IOP. The amplitude of the variation is 0.6°K. Again, there is a distinctive afternoon maximum. The diurnal cycle in $\overline{\theta}_v$ at the *Moana Wave* (Figure 7.7) is very similar to that at Kapinga; however, the amplitude of the variation is 0.3°K -- half the

amplitude of the $\overline{\theta}_v$ variation at Kapinga. This difference may be in part attributed to possible heat island effects at the Kapinga atoll.

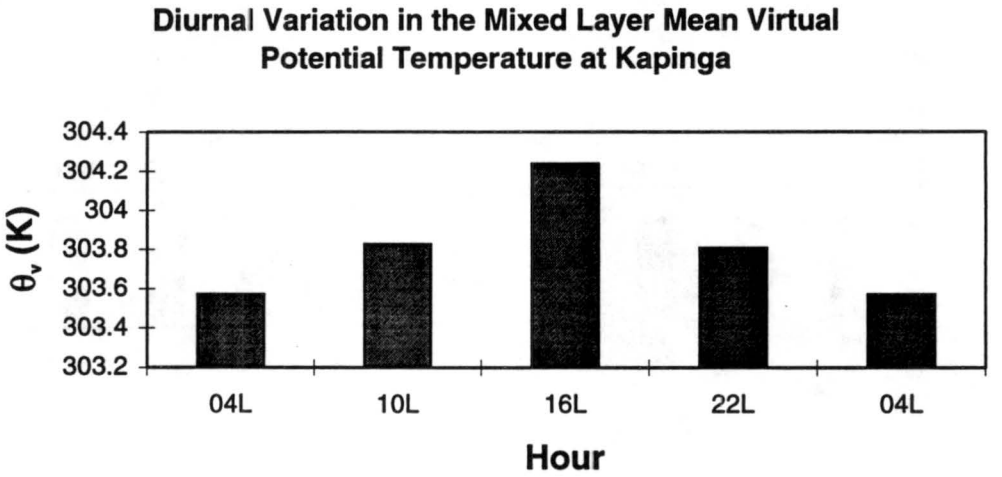

Figure 7.6 Diurnal variation in $\overline{\theta}_v$ at Kapinga.

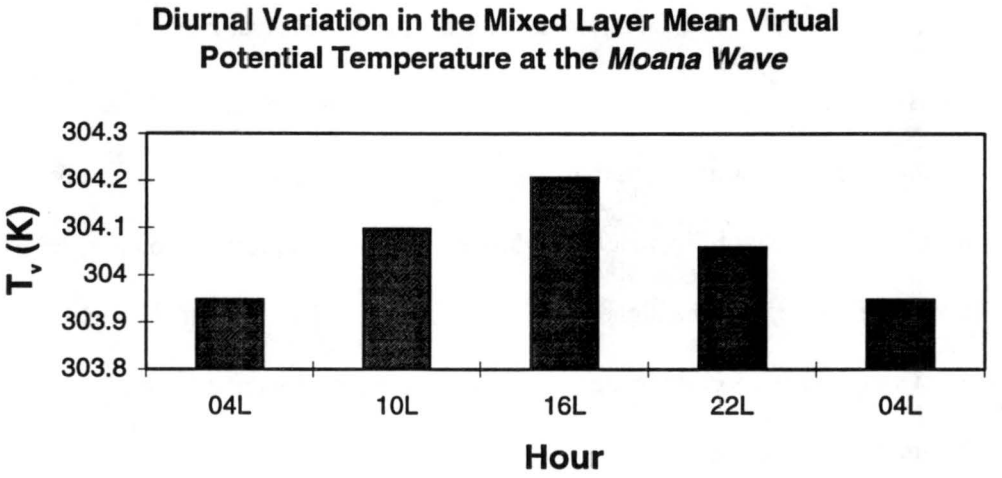

Figure 7.7 Diurnal variation in $\overline{\theta}_v$ at the *Moana Wave*.

Recall from (4.1) that the buoyancy flux, which affects the mixed layer depth, is related to the sensible and latent heat fluxes. Figure 7.8 shows the diurnal cycle in both surface fluxes at the IMET buoy. These fluxes will be combined in Section 7.6 to produce the buoyancy flux diurnal cycle, which will then be used in a thermodynamic budget of the mixed layer

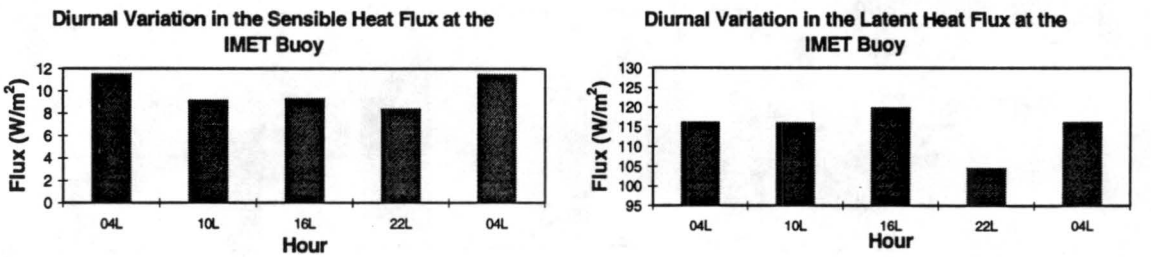

a. b.

Figure 7.8 Diurnal variation in the sensible (a) and latent (b) heat fluxes at the IMET buoy.

The height of the LCL (computed from the mixed layer mean θ and q) at Kapinga also varies diurnally (Figure 7.9). The shape of the LCL variation closely resembles that of $\overline{\theta}_v$ (Figure 7.6). Both warming and drying cause the LCLs to be deeper in the afternoon; however, there is also the possibility that the nighttime maximum in precipitation may be contributing to lower LCLs at night. The higher LCLs at 16L suggest that the cloud base rises in the afternoon, but evidence to support this suggestion is not available. This pattern might reflect the nighttime maximum in precipitation.

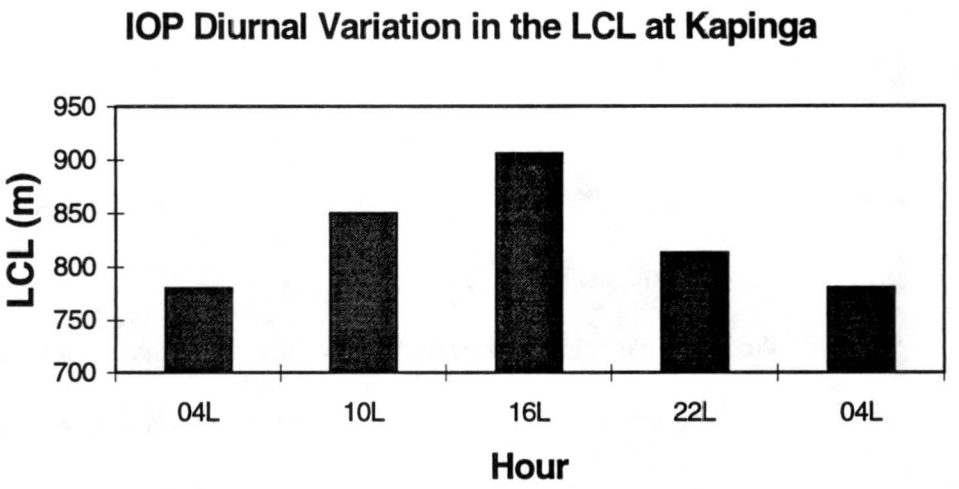

Figure 7.9 Diurnal variation in the LCL at Kapinga for the IOP.

7.4 Dependence on Sky Conditions

Hourly Geostationary Meteorological Satellite (GMS) brightness temperature data (courtesy of Dr. Tetsuo Nakazawa) and IR satellite images to were used to quantify sky conditions. The satellite data have a spatial resolution of approximately 11 km (Lin and Johnson 1996). Data at each pixel were first averaged to get values in a 1° grid box. A program created by Pat Haertel (personal communication, 1996) then averaged the gridded data in a specified range within the IFA. For the brightness temperatures used in this analysis, we chose a two degree by two degree box centered on Kapinga and the IMET buoy.

Comparing the satellite images of the IFA and the brightness temperatures at Kapinga, we determined the sky condition every 6 hours. A day labeled "clear" had no visible clouds at any one of the 4 reporting times. Days that were cloudy half of the day and clear the rest were not included as either cloudy or clear.

Figure 7.10 illustrates the diurnal dependence of mixed layer properties on sky conditions. The figure shows the average daily variation in both z_i and $\overline{\theta}$ for clear and cloudy skies for winds less than 3 m/s. Strong winds promote mixing that can obscure the diurnal cycle

and thus they were not included in this analysis. Diurnal variation is the greatest on days with clear skies and light-winds. The deepest mixed layer for the clear sky case occurs at 16L with a top of 938.7 mb (627.4 m) while the shallowest mixed layer is at 10L (948.2 mb or 538.7 m). Thus, the depth varies approximately 16.5% for the clear case. Note that these deeper mixed layers also correspond to higher values of $\overline{\theta}$.

Light-wind days with cloudy skies have an average z_i ~14 mb lower (~128 m shallower) than those days with clear skies. Furthermore, the mean θ on cloudy days is ~0.5° C cooler (due to less radiational heating and possible convective effects) which is consistent with the shallower mixed layers. For clear skies at Kapinga, $\overline{\theta}$ varies by ~1° C over the course of the day (comparable to Weller and Anderson (1995) who found the amplitude in the diurnal variation in SST during moderate to low wind speeds to be 0.5 to 2.0°C), whereas under cloudy skies $\overline{\theta}$ varies by approximately 0.5° C. Both cases have the maximum in both z_i and $\overline{\theta}$ occurring in the afternoon (16L). The clear/cloudy sky diurnal data are listed in Table 7.1.

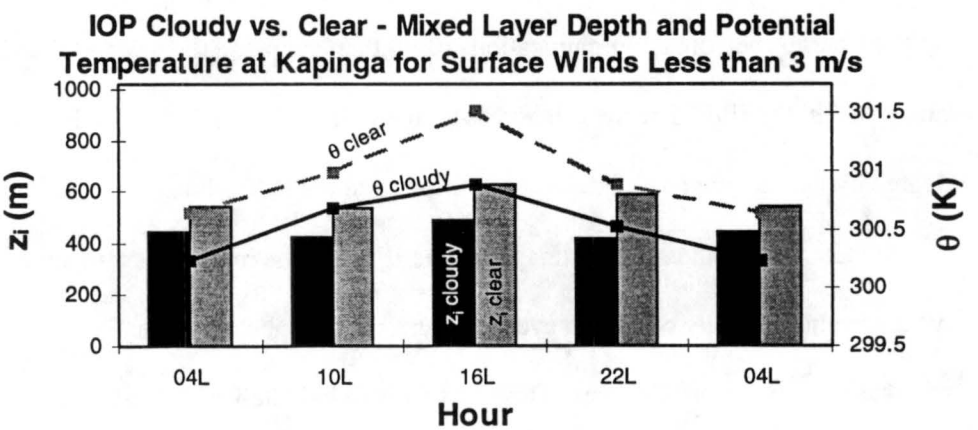

Figure 7.10 Diurnal variation in z_i and $\overline{\theta}$ at Kapinga for cloudy and clear sky conditions for winds less than 3 m/s. Vertical bars represent the mixed layer depth (dark for cloudy skies, light for clear); lines represent potential temperature (dark for cloudy skies, light for clear).

	z_i cloudy	z_i clear	θ cloudy	θ clear
04L	958.6 mb (442.6 m)	948.1 mb (539.7 m)	300.2	300.6
10L	960.3 mb (427.0 m)	948.2 mb (538.7 m)	300.7	301.0
16L	953.6 mb (488.7 m)	938.7 mb (627.4 m)	300.9	301.5
22L	961.3 mb (417.9 m)	943.2 mb (585.3 m)	300.5	300.9

Table 7.1 Cloudy versus clear diurnal data at Kapinga for winds less than 3 m/s (corresponding to Figure 7.10)

Since the diurnal variation is greatest on clear, light-wind days, it is interesting to plot the diurnal variation for a specified light-wind period. From November 27 - December 7, the mean surface wind speed at Kapinga was 1.1 m/s. Figure 7.11 shows that for this time interval the mixed layer top displays almost an ideal diurnal cycle with a day-to-night variability of 160.7 m. This result plus those in Figure 7.10 show that a diurnal cycle of z_i can occur due to surface heating alone, i.e., the earlier diurnal cycle results for the entire IOP were not simply due to more rain at night.

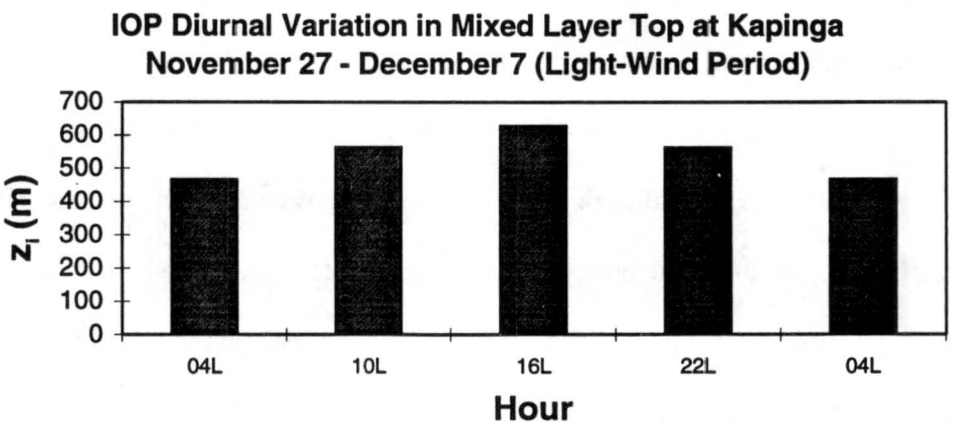

Figure 7.11 Diurnal variation in the mixed layer top at Kapinga for November 27 - December 7 (light-wind period).

7.5 Diurnal Variation in the Mean Structure

To study the diurnal variation in the mixed layer structure we created mean IOP soundings at Kapinga for 18 UTC (04L), 00 UTC (10L), 06 UTC (16L), and 12 UTC (22L) (Figure 7.12a, b, c, d). Differences from Figure 7.1 arise from variations in the surface pressure that factors into the scaled soundings but not into plots of just the mixed layer top. Notice how the mixed layer is substantially deeper in the afternoon (559 m at 16L) and shallowest in the early morning (497 m at 04L). Furthermore, the mixed layer is warmest at 16L (~301.2°K), over a half-degree warmer than at 04L (~300.6). Although little emphasis has been place on surface values (especially the surface moisture), these soundings show evidence of a nocturnal inversion at Kapinga with θ varying approximately 2°K from 04L to 16L. The surface layer becomes stably stratified at night with the atoll warming up during the day.

The most noteworthy differences in the soundings are the variations in z_i and θ. Specific humidity varies little on the diurnal time scale with the afternoon sounding slightly drier. Each shows a well-mixed structure in both θ and q. As we detected in the overall mean soundings, θ begins to increase and q begins to decrease approximately 50 m below z_i. Above z_i there is evidence of an entrainment zone roughly 100 m deep.

Bond found that the mixed layer in the eastern equatorial Pacific also exhibits a diurnal variation (Bond 1992), although the data set was acknowledged to be limited. He found the amplitude of the diurnal temperature cycle is greater for the atmospheric mixed layer than for the SST. Furthermore, the mixed layer tended to be more shallow and slightly more stably stratified at night than during the day. A slight increase in the stability of the mixed layer at night was also noted over the warm pool (Figure 7.12a).

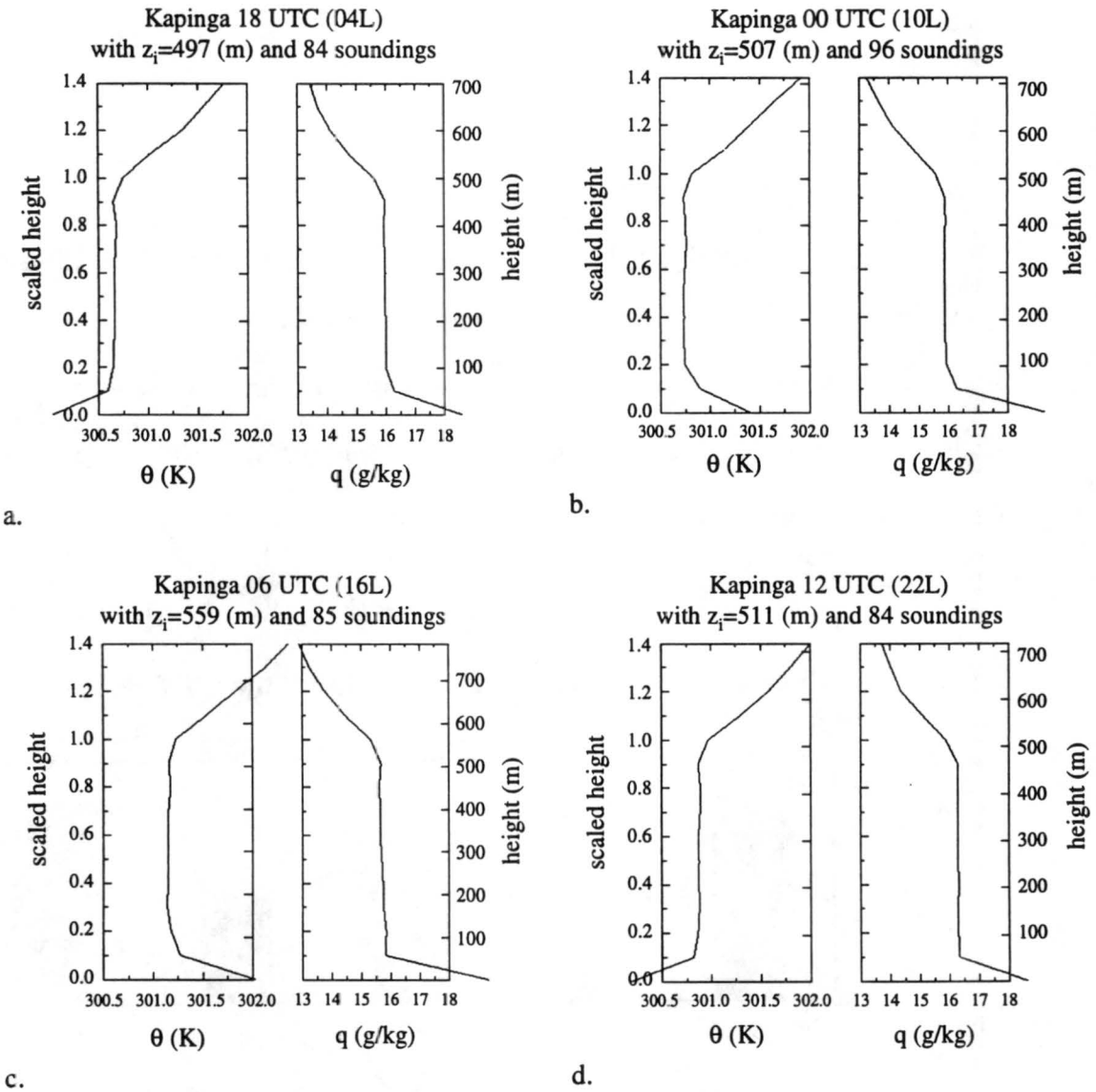

Figure 7.12 The diurnal cycle in the mean structure at Kapinga for the IOP. 18 UTC, 06 UTC, 12 UTC, and 00 UTC are shown in panels a, b, c, and d respectively.

7.6 Mixed Layer Budget Results

Recall from (4.7) that the change in $\overline{\theta}_v$ with time is equal to the difference in the heat fluxes at the top and bottom of the mixed layer divided by the mixed layer top plus an additional term for radiative cooling. Again using the closure $F_i = -kF_s$, (4.7) can be written:

$$\frac{\partial \overline{\theta}_v}{\partial t} = \frac{(1+k)F_s}{z_i} + Q_{Rm} \tag{7.1}$$

Using the change in $\overline{\theta}_v$ and mixed layer top at Kapinga with the buoyancy flux at the IMET buoy (Figure 7.13), we can solve (7.1) for the mixed layer mean radiative heating rate Q_{Rm}. Ideally, this computation is best for clear sky conditions. However, as a first attempt, we will use the IOP mean values in the calculations. According to Stull (1976), $k = 0.2$ is a good average for free convection where the buoyancy force is dominant.

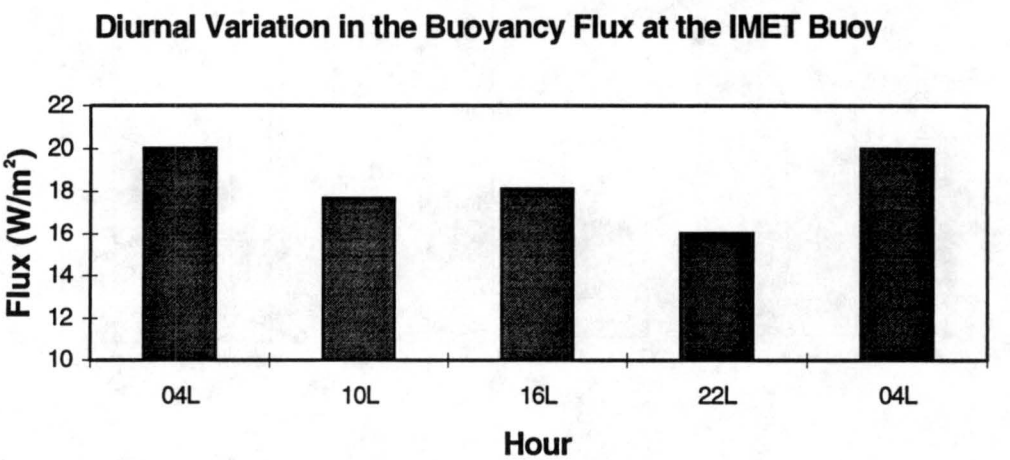

Figure 7.13 The diurnal variation in the buoyancy flux at the IMET buoy.

According to Figure 7.6,

$$\frac{\partial \overline{\theta}_v}{\partial t} = \frac{0.6^o K}{12h} = 1.2\frac{^o K}{day} \tag{7.5}$$

for the time period 04L to 16L. This quantity is positive during the day (04L to 16L) and negative during the night (16L to 04L). Using the daytime midpoint values (10L) for the IMET

buoy buoyancy flux and the height of the mixed layer at Kapinga, (7.1) yields Q_{Rm} = -1.7°K/day. During the night (16L to 04L), the same calculation gives Q_{Rm} = -3.8°K/day.

Although Kapinga is a very small atoll, the relatively large variation in $\overline{\theta}_v$ suggests that there is some evidence of a heat island effect. For comparison, we can repeat the above calculations for the *Moana Wave*. From 04L to 16L,

$$\frac{\partial \overline{\theta}_v}{\partial t} = \frac{0.3^o K}{12h} = 0.6 \frac{^o K}{day}$$

Note that this is half of the variation in $\overline{\theta}_v$ observed at Kapinga. Using again the IMET buoy buoyancy flux data and the mixed layer top from Figure 7.2b, we can solve for the day and night radiational cooling at the *Moana Wave*:

Q_{Rm} = -2.28°K/day (during the day)

Q_{Rm} = -3.24°K/day (during the night)

Although the day-to-night difference in the radiative cooling of ~1°K/day is less at the *Moana Wave* where there is a smaller diurnal variation in $\overline{\theta}_v$, the daily mean value for Q_{Rm} is the same at both sites, -2.8°K/day. The daily average of -2.8°K/day and day-to-night variation in Q_{Rm} are in good agreement with computations currently being conducted by Dr. Graeme Stevens (personal communication, 1996). These comparisons will be reported shortly in a separate paper.

This study shows that there is definitely a diurnal cycle in the mixed layer depth and thermodynamic variables over the western Pacific warm pool. In general, the mixed layer is deepest in the afternoon when the surface fluxes are maximum. Convective downdrafts modify ambient conditions and create shallower mixed layers. This alteration frequently, but not always, interrupts the diurnal cycle. Strong winds also inhibit diurnal variation of SST (Weller and

Anderson 1995). Therefore, diurnal variation is the greatest on clear, light-wind days. Mean mixed layer soundings show an increase in virtual potential temperature and mixed layer depth from 04L to 16L. The specific humidity varies less but the deep afternoon mixed layers tend to be drier, especially at Kapinga. This pattern of deep, dry mixed layers was not evident at the *Moana Wave*; however, like Kapinga, the amplitude of the q variation was relatively small. A thermodynamic budget for the mixed layer yielded a mixed layer mean radiative cooling of -2.8°K/day, with a day-to-night variation of ~1°K/day. Work is currently underway to relate this result to independent computations based on longwave and shortwave radiative models (Graeme Stephens, personal communication 1996).

Chapter 8

SUMMARY AND CONCLUSIONS

The ultimate objective of TOGA COARE was to improve air-sea interaction and boundary layer parameterizations in models of the ocean and the atmosphere (Webster and Lukas 1992). A better understanding of the atmospheric mixed layer over the warm pool is an essential factor in this quest since the actual coupling occurs through the ocean and atmospheric mixed layers.

In this study, we analyzed the atmospheric mixed layer over the warm pool. IOP time series of several variables were analyzed to study long-term variability of the mixed layer. A low-frequency variation was apparent in the IOP time series of mixed layer tops at Kapinga. This fluctuation suggests a connection to the 40-50 day oscillation. A comparison of the time series of the buoyancy flux at the IMET buoy and the mixed layer tops at Kapinga did not correlate well. Theoretically, a large buoyancy flux should result in a deeper mixed layer. This behavior was seldom observed suggesting that the simple one-dimensional mixed layer model is not sufficient to simulate mixed layer response for the entire TOGA COARE IOP. The frequent convection over the western Pacific warm pool disrupts the mixed layer enough to invalidate the model. However, the model should work well during undisturbed periods. In practice it is difficult to apply the model due to the complexity in computing accurate values of large-scale vertical motion at the mixed layer top.

At Kapinga, high surface wind speeds tended to correspond to shallow mixed layers. This correlation may have been the result of cold downdrafts from convective systems which will

momentarily increase the surface wind speed but confine mixing to shallow layers. The time series of precipitation at Kapinga showed shallower mixed layer tops when rain was occurring. Furthermore, three westerly wind bursts occurred during the four-month IOP. These strong-wind events had a definite impact on the state of the boundary layer.

We presented histograms to illustrate the range of mixed layer tops. The distribution of z_i at Kapinga and *Ship 3* were skewed toward shallower values. This suggests the presence of convective downdrafts that destroy or suppress the mixed layer as cold, stable air hits the ocean surface. The distribution of z_i at *Ship 5* and the *Moana Wave* did not exhibit this apparent skewness. Histograms of mixed layer tops were also created for light- and strong-winds at the surface. The light-wind cases showed a more normal distribution which probably resulted from filtering out the effects of convective wakes.

Scatterplots of θ and q versus mixed layer top showed that for θ less than 301°K there was a positive correlation between the mean potential temperature in the mixed layer and the depth of the mixed layer. Precipitation was often occurring when the mixed layer tops were the lowest. There was a weak negative correlation between mixed layer tops and q. This tendency would correspond to the entrainment of drier air from aloft.

Mean thermodynamic profiles were created at four different TOGA COARE sounding stations. The resulting structures were consistent at each site, namely, each showed a well-mixed structure in both θ and q capped by an entrainment zone. The height of the mixed layer top varied somewhat from station to station with the lowest at 470 m (*Ship 3*) and the highest at 540 m (*Ship 5*). These heights are comparable to results from the Atlantic (424 m, Fitzjarrald and Garstang 1981) and the eastern equatorial Pacific (~500 m, Bond 1992). Therefore, from this study we conclude that the mixed layer tops over the warm pool are similar to those reported throughout the maritime tropics.

This study also showed that the mixed layer depth over the warm pool exhibits diurnal variations. At Kapinga, the diurnal variation in mixed layer top, potential temperature, specific humidity, and LCL were analyzed. Diurnal cycles were also identified at the *Moana Wave*, *Ship 3*, and *Ship 5*. In each case, the deepest and warmest mixed layers occurred in the afternoon (16L). The variation in the mixed layer top was analyzed for light-wind cases and for clear versus cloudy sky conditions. The largest diurnal variations were found on days with light-winds and clear skies. Examination of mean profiles for 00 UTC, 06 UTC, 12 UTC, and 18 UTC showed that the same well-mixed profile found in the overall mean sounding persisted for each time division. Again, the profiles showed a dependence on radiational heating being the warmest and the deepest in the afternoon and the coolest and shallowest in the night/early morning.

The mixed layer mean thermodynamic budget was solved yielding the net radiative heating of the mixed layer Q_{Rm} as a residual. The mean value of Q_{Rm} is -2.8°K/day, although a diurnal cycle of amplitude ~1°K/day is diagnosed with the weakest cooling in the afternoon -- suggesting important contributions by shortwave absorption during the day. These findings compare well with recent independent computations by Dr. Graeme Stephens (personal communication, 1996).

Beside the warm SSTs, the TOGA COARE data set is unique in that it allows us to study the atmosphere over the equator. Traditional theory says that the atmospheric boundary layer over the equator must be very deep due to the warmer SSTs and reduced subsidence. Ekman theory also predicts an infinitely deep boundary layer on the equator where the Coriolis parameter equals zero. However, this study supports the work of Gray (1972) and Schubert et al. (1995) who found no substantial increase in the thickness of the boundary layer towards the equator.

We have analyzed various aspects of the atmospheric mixed layer over the warm pool revealing some insightful results. To further our understanding in this area, additional research is

necessary. For example, as a refinement to the mean soundings in Chapter 6, scaled plots could be created for those soundings where the top of the entrainment zone could be identified. Also, sounding data used in this analysis could be compared to the Radio Acoustic Sounding System (RASS, Parsons et al. 1994) or aircraft data also available from TOGA COARE. The inability to calculate the mean vertical motion at the top of the mixed layer made it difficult to test the simple mixed layer model of Tennekes (1973) for undisturbed periods. However, with some caution, it may be applied to several carefully selected light-wind periods and to the study of diurnal variations. Finally, the atmospheric mixed layer is only half of the ocean-atmosphere coupling. Atmospheric findings must be related to the oceanic mixed layer to fully comprehend the coupling between the two systems. Of notable interest would be to compare the diurnal evolution of the atmospheric mixed layer to that of the ocean.

REFERENCES

Augstein, E., H. Schmidt, and R. Ostapoff, 1974: The vertical structure of the atmospheric planetary boundary layer in undisturbed trade winds over the Atlantic Ocean. *Bound. Layer Meteor.*, **6,** 129-150.

Barnes, G.M. and M. Garstang, 1982: Subcloud layer energetics of precipitating convection. *Mon. Wea. Rev.*, **110,** 102-117.

Betts, A.K., 1976: Modeling subcloud layer and interaction with a shallow cumulus layer. *J. Atmos. Sci.*, **33,** 2363-2382.

Bolton, D., 1980: The computation of equivalent potential temperature. *Mon. Wea. Rev.*, **108,** 1046-1053.

Bond, N.A., 1992: Observations of Planetary Boundary-Layer Structure in the Eastern Equatorial Pacific. *J. Clim. Appl. Meteor.*, **5,** 699-706.

Cole, H., 1993: The TOGA COARE ISS radiosonde temperature and humidity sensor errors. National Center for Atmospheric Research, Tech. Report Oct. 1993, 26 pp.

Fairall, C.W., E.F. Bradley, D.P. Rogers, J.B. Edson, and G.S. Young, 1996: Bulk paramaterization of air-sea fluxes for TOGA COARE. *J. Geophys. Res.* (submitted).

Fitzjarrald, D.R. and M. Garstang, 1981: Vertical structure of the tropical boundary layer. *Mon. Wea. Rev.*, **109,** 1512-1526.

Gaynor, J.E. and C.F. Ropelewski, 1979: Analysis of the convectively modified GATE boundary layer using *in situ* and acoustic sounder data. *Mon. Wea. Rev.*, **107,** 985-993.

Gray, W. M, 1972: A diagnostic study of the planetary boundary layer over the oceans. Department of Atmospheric Science Colorado State University Paper No. 179, 95 pp.

Gray, W.M. and R.W. Jacobson Jr., 1977: Diurnal variation of deep cumulus convection. *Mon. Wea. Rev.*, **105,** 1171-1188.

Holland, J.Z. and E.M. Rasmusson, 1973: Measurements of the atmospheric mass, energy and momentum budgets over a 500-kilometer square of tropical ocean. *Mon. Wea. Rev.*, **101,** 44-45.

Houze, R.A., 1977: Structure and dynamics of a tropical squall line system. *Mon. Wea. Rev.*, **105,** 1540-1567.

Johnson, R.H., 1977: Effects of cumulus convection on the structure and growth of the mixed layer over south Florida. *Mon. Wea. Rev.*, **105,** 713-724.

Johnson, R.H. and M.E. Nicholls, 1983: A composite analysis of the boundary layer accompanying a tropical squall line. *Mon. Wea. Rev.*, **111,** 308-319.

Johnson, R.H. and P.J. Hamilton, 1988: The relationship of surface pressure features to the precipitation and airflow structure of an intense midlatitude squall line. *Mon. Wea. Rev.*, **116,** 1444-1472.

Johnson, R.H., P.E. Ciesielski, and K.A. Hart, 1995: Tropical inversions near the 0°C level. *J. Atmos. Sci.* (submitted).

LeMone, M.A. and W.T. Pennell, 1976: The relationship of trade wind cumulus distribution to subcloud layer fluxes and structure. *Mon. Wea. Rev.*, **104,** 524-539.

Lin, X. and R.H. Johnson, 1996: Kinematic and thermodynamic characteristics of the flow over the western Pacific warm pool during TOGA COARE. *J. Atmos. Sci.*, **53,** 695-715.

Loehrer, S.M., T.A. Edmunds, and J.A. Moore, 1995: TOGA COARE upper-air sounding data archive: development and quality control procedures. *J. Atmos. Sci.* (submitted).

Madden, R.A. and P.R. Julian, 1972: Description of global-scale circulation cells in the tropics with a 40-50 day period. *J. Atmos. Sci.*, **29,** 1109-1123.

Mahrt, L., 1976: Mixed layer mean structure. *Mon. Wea. Rev.*, **104,** 1403-1407.

Mapes, B.E. and P. Zuidema, 1996: Radiative-dynamical consequences of dry tongues in the tropical troposphere. *J. Atmos. Sci.*, **53,** 620-638.

Miller, E.R. and A.C. Riddle, 1994: TOGA COARE Integrated Sounding System Data Report - Vol. IA Revised Edition, 59 pp.

Parsons, D., W. Dabberdt, H. Cole, T. Hock, C. Martin, A. Barrett, E. Miller, M. Spowart, M. Howard, W. Ecklund, D. Carter, K. Gage, and J. Wilson, 1994: The integrated sounding system: description and preliminary observations from TOGA COARE. *Bull. Amer. Meteor. Soc.*, **75,** 553-567.

Petersen, W.A., S.A. Rutledge, and R.E. Orville, 1996: Cloud-to-ground lightning observations from TOGA COARE: selected results and lightning location algorithms. *Mon. Wea. Rev.*, **124,** 602-620.

Press, W.H., S.A. Teukolsky, W.T. Vetterling, and B.P. Flannery: 1992, *Numerical Recipes in FORTRAN.* Cambridge University Press, New York, 963 pp.

Rickenbach, T. 1995: Rainfall production from the spectrum of convection observed by shipboard radar during TOGA COARE. Preprints, 21st Conference on Hurricanes and Tropical Meteorology, Amer. Meteor. Soc., Miami, FL.

Rutledge, S.A. and R.A. Houze Jr., 1987: A diagnostic modeling study of the trailing stratiform region of a midlatitude squall line. *J. Atmos. Sci.,* **44,** 2640-2656.

Schubert, W.H., P.E. Ciesielski, C. Lu, and R.H. Johnson, 1995: Dynamical adjustment of the trade wind inversion layer. *J. Atmos. Sci.,* **52,** 2941-2952.

Smull, B.F. and R.A. Houze Jr., 1985: A midlatitude squall line with a trailing region of stratiform rain: radar and satellite observations. *Mon. Wea. Rev.,* **113,** 117-133.

Stull, R.B., 1976: Mixed layer depth model based on turbulent energetics. *J. Atmos. Sci.,* **33,** 1268-1278.

Stull, R.B.: 1993, *An Introduction to Boundary Layer Meteorology.* Kluwer Academic Publishers, Dordrecht, 666 pp.

Tennekes, H., 1973: A model for the dynamics of the inversion above a convective boundary layer. *J. Atmos. Sci.,* **30,** 558-567.

Velden, C.S. and J.A. Young, 1994: Satellite observations during TOGA COARE: large-scale descriptive overview. *Mon. Wea. Rev.,* **122,** 2426-2441.

Wang, T., K.B. Earnshaw, and R.S. Lawrence, 1979: Path-averaged measurements of rain rate and raindrop size distribution using a fast-response optical sensor. *J. Appl. Meteor.,* **18,** 654-660.

Webster, P.J. and R. Lukas, 1992: TOGA COARE: the coupled ocean-atmosphere response experiment. *Bull. Amer. Meteor. Soc.,* **73,** 1377-1416.

Weller, R.A. and S.P. Anderson, 1995: Surface meteorology and air-sea fluxes in the western equatorial Pacific during the TOGA Coupled Ocean Atmosphere Response Experiment. *J. Climate* (submitted).

White, A.B. and C.W. Fairall, 1996: Shipboard measurements of convection during COARE. Preprints, Eighth Conference on Air-Sea Interaction, Amer. Meteor. Soc., Atlanta, GA.

Young, G.S. and S.M. Perugini, 1995: Convective wakes in the equatorial western Pacific during TOGA. *Mon. Wea. Rev.,* **123,** 110-123.

Zipser, E.J., 1977: Mesoscale and convective-scale downdrafts as distinct components of squall-line structure. *Mon. Wea. Rev.,* **105,** 1568-1589.